

Functional Sustainability of a Flight Dynamics Control System for Stable Hovering Flight of an Unmanned Aerial Vehicle (UAV), such as in Agricultural Applications: Mathematical Modeling and Simulation

Naji Mordi Naji Al-Dosary

Department of Agricultural Engineering, College of Food & Agriculture Sciences, King Saud University, Riyadh, P.O. Box 2460, Riyadh 11451, KSA

Abstract: The simulation of a control system for the longitudinal axis of the rotary or fixed-wing unmanned aerial vehicles (UAVs) is demonstrated in this study. The control unit includes design considerations of two controllers to provide robust stability, tracking of the proposed linear dynamics, an adequate set of proportional-integral-derivative (PID) controller gains, and a minimal cost function. The PID control and linear quadratic regulator (LQR) with or without full-state-observer were evaluated. An optimal control system is assumed to provide fast rise and settling time, minimize overshoot, and eliminate the steady-state error. The effectiveness of this approach was verified by a linear model of the UAV aircraft in the semi-dynamic simulation platform of Matlab/Simulink, in which the open-loop system was assessed in terms of flight robustness and reference tracking. The experimental results show that the proposed controllers effectively improve the configuration of the control system of the plant, maintain the sustainability of the dynamic flight model stability, and diminish the flight controller errors. The LQR provides robust stability, but it is not optimal in the transient phase of particular plant output. The PID control system can adjust the controller's gains for optimal hovering (or stable slow flight) and is especially useful for the tracking system. Finally, comparing aircraft stability using PID and LQR controllers shows that the latter has less overshoot and a shorter settling time; in addition, all proposed controllers can be practically deployed as one UAV's system, which can be handled as an exemplary model of the UAV flight management system.

Key words: Agricultural applications, cost function, dynamic model, PID & LQR controllers, steady-state error, UAV aircraft.

1. Introduction

This article initially considers the simulation of an aircraft movement control system, specifically the control of a longitudinal maneuver of unmanned aerial vehicles (UAVs) through the use of a proportional-integral-derivative (PID) controller and a linear quadratic regulator (LQR) controller, and is also consistent with other agriculture applications and performance of the entire UAV aircraft control systems that were studied in previous scientific researches and were discussed as literature studies in this article as detailed below.

1.1 A Brief History of UAVs in Agriculture Applications

Systems studies, research, and development to apply modern technology to applications in agricultural activities are moving ahead at a rapid pace. Practical applications of UAVs—drones have been in use since the 1980s, and durable drone technology has arrived, especially in agriculture strategies based on real-time data processing [1]. Agricultural drones for agriculture field operations, e.g., economics-based strategy for either agricultural cycle or crop cycle, such as field spraying by UAV, are the best technology model currently being utilized for advancing agricultural

Corresponding author: Naji Mordi Naji Al-Dosary, Ph.D., associate professor, research fields: farm power and machinery engineering.

production. Norasma *et al.* [2] indicated that the current deployment of UAVs and associated applications in agriculture support their continued use to properly manage farms for increased agricultural efficiency and productivity of cultivated plants, a pest control application, and geographic information system (GIS) and image processing of agriculture fields.

Tokekar *et al.* [3] studied remote sensing and soil sampling practice and methodology through the application of a coalition of an UAV and an unmanned ground vehicle (UGV) for precision agricultural applications. This study estimated soil nitrogen (N) levels based on the combination of ground and aerial measurements and created a map of these levels throughout the studied farm field for optimal fertilizer use. Their study provided a method for determining if each spot on the field, which was being covered with compost, had less than the permissible minimum nitrogen level, and thus would be less likely to be misclassified. In addition, choosing an operating approach such as tuning the paths of the aircraft tours above each spot of the farm field would minimize the UAV operation time for measurement of the fertilizer levels and allow for longer aircraft battery life. The main points of their study were whether the use of fertilizers could be significantly different from what would be expected, and total usage could be drastically reduced. The technical applications of unmanned vehicles would minimize the UAV operation time for measurements of the fertilizer levels. Additionally, the use of both UAV and UGV systems and associated simulations clearly helped to reduce the number of potentially mislabeled (PML; per soil nitrogen (N) percentage) field spots as compared to only using the UAV system. This was accomplished through the use of the clearly defined system parameters and actual collected soil measurements from the spots on the agricultural field.

Field performance and application of pesticide spray by UAV aircraft systems can provide an opportunity for a highly specific and precise spatial distribution of

pesticide in spray applications, especially in varied topographies. In California, a UAV aircraft (Helicopter model RMAX, Yamaha Motor Co., USA) with a crop chemical spray system was utilized via a remote control unit, to control the maneuvers of the UAV aircraft, for spraying 0.61 ha of grape fields (42 rows by 61 m long with 2.4 m spacing of rows). Depending on the mounted swath width of the aircraft sprayer, pesticide application of 2.0 to 4.5 ha/h and volume rates of 14 to 39 L/ha could be achieved. The volume rates of pesticide, when applied by the UAV aircraft, achieved increased chemical-drizzles precipitation on the leaves of the crop. When comparing two methods of application, traditional ground sprays required a volume rate of 935 L/h to achieve chemical-drizzles precipitation on the leaves equivalent to UAV system application at 47 L/ha [4].

Ju and Son [5] indicated that increasing field operation efficiency and reducing time lost by operators of conventional agriculture mechanization could be accomplished through the use of the modern UAV operating systems. The UAV aircraft system generally employed in agriculture was a single UAV with a controller unit. But, Ju and Son also compared various quadcopter-type UAV aircraft systems including: a UAV with an independent control unit, a UAV with a remote control unit, multiple UAVs with independent control units, and multiple UAVs with remote control units. Among the performance variables measured for this study are total journey time, consumption of battery energy, and landing area inaccuracy. Agricultural field performance results indicated that multiple UAVs aircraft systems, could solve the problem of energy consumption and battery shortage, increase the field performance, and reduce operation and control time to less than 66.1% (from 96.2 s to 32.6 s), of either of the single UAV aircraft systems. However, their results also noted distance and accuracy of landing differences; the landing distance was higher for the multiple UAVs aircraft (19.3 cm) compared to the single UAVs aircraft (8.3 cm).

Hasan *et al.* [6] have devoted their research to develop and demonstrate a fixed-wing, aircraft type portable drone with different capabilities depending on the configuration. The drone is suitable for agricultural applications with the potential of flying at various altitudes from 10 to 200 m, a maximum cruise speed of 60 km/h, and the capability of a payload of 1.4 kg, e.g., seeds or emergency supplies to field workers. The portable aircraft can be configured with a loud-speaker to frighten birds, and a high-definition camera to broadcast live video of any crop field, for monitoring possible crop damage from plant diseases or destruction by birds or other animals. In addition, UAV technology can be used for further advances in agricultural crop service applications, such as fertilizers, pesticides, and irrigation water applications, as well as significant operating efficiencies, reduced production costs of agricultural crops and labor demand [7]. Yuan *et al.* [8] study indicated the ability of UAVs to accurately assist in the photogrammetry of apple orchards density variations and that future studies should consider the accuracy of measurement techniques given varying image qualities and the UAVs flight settings and design.

Potential requirements and major challenges to increase future food production involve the deployment of modern communications and remote technology services, offering the ability to increase the productivity of agro-products and automate agrochemical applications such as pesticides and fertilizers, thus minimizing the cost of field operations. Integrating the technical capabilities of UAVs for agricultural operations, specifically remote sensors and wireless communications or precision spray applications, along with smart agriculture applications, such as soil mapping, or aerial crop monitoring and production mapping via global positioning system (GPS) and GIS systems can yield significant results. Maximizing the utility of these advanced UAVs offers promising results for the future, but it requires consideration of multiple factors (advantages/limitations) inherent in UAVs, such as

flying direction, propellers' velocity, thrust forces, landing and takeoff flexibility, bulk payload, endurance, battery capabilities, etc. [9].

1.2 A Brief History of Robust Control Systems in UAVs

Automatic control systems impact many aspects of life in advanced civilizations today, but especially in aeronautical applications. Efficiency in control systems has particularly enhanced the stability of aircraft in flight. A reconfigurable flight control system depends on the proper functioning of the large number of control systems used in any aircraft. There are two types of automated control systems. The first is an open-loop control system in which the output quantities have no influence on the input quantities. The second system is known as closed-loop control, where the output has an effect upon the input quantities, which produces a control feedback action. The best example to describe that control system is the modern aircraft flight control system where input parameters and output are displayed on the aircraft control panel. Studies have shown that modern control systems will benefit many aspects of society.

Chen *et al.* [10] indicated that an adaptive feedback linear control model for an aircraft maneuvering in a large-angle rotation (pitch angle) could only suppress the vibration of the aircraft when hovering. Their model measured the system input, output variable (pitch angle), and time derivatives. These measures can also ensure that the steady-state error in pitch control (pitch angle) is equal to zero. In addition, the simulation results compared feedback of linear control and adaptive control in structure variables, showing that the adaptive feedback linear control is superior in resistance to external disturbances of the system model and improves reliability and adaptability of the aircraft attitude control systems.

Salih *et al.* [11] developed a robust dynamic model for a stable and accurate controller of an actuated UAV aircraft with four fixed pitch angle rotors. The PID controller system was developed for stability in flight

obtained by changing the pitch, roll, and yaw angles. This study predicted a model with 4 forces, one for each UAV propeller connected to each of four rotors at a fixed angle. Results have shown that forward or backward motion of the aircraft is accomplished by increasing or decreasing the speed of the front and rear rotor speed; decreasing rear rotor speed in opposition to increasing front rotor speed (or vice versa) will affect the pitch angle. The roll angle will be changed in a similar manner to using the two lateral rotors to achieve aircraft motion right or left. To achieve the yaw angle, the speed of the front and rear counter-clockwise rotating propellers would be increased or decreased while the other two motors' clockwise rotating propeller speeds are decreased or increased in opposition.

A dynamic model of a quadcopter with PID and LQR controllers for 10 attitudes was studied by Argentim *et al.* [12]. This research indicated that the best simulation results were obtained for the vertical attitude. Three different control systems were used to control the UAV platform: PID controller, LQR, and a PID with an LQR loop. The results showed that the LQR controller gave a very low steady-state error, but the PID controller gave a perfect response. However, the PID with the LQR controller offered an inferior performance of the UAV with a delayed response when compared to the other controllers, but from a practical standpoint, the PID with an LQR controller was easily implementable and robust.

Noshahri and Kharrati [13] indicated that the UAV's performance and its dynamic motions can be enhanced by improving the PID controller. Noshahri and Kharrati proposed and developed a controller with 6 degrees of freedom (DOF) that used a nonlinear algorithm (genetic algorithm) to determine the PID controller gains for optimum performance of the UAVs. Although the PID controller and algorithm found suboptimal coefficients, simulation results are presented that verify the effectiveness of the proposed control system and performance of the closed-loop control system as

compared to the flight performance with controller system coefficients of previous studies.

Khatoon *et al.* [14] presented a study of the different control models: PID and LQR controllers utilized in the dynamic model of a Quadrotor UAV platform. Results showed that the PID controller could be utilized for its versatility, easy execution, and provided a perfect response to the model dynamic attitudes. The LQR controller was perfect for the controller comparison due to its performance robustness. Both PID and LQR controllers provided effective results that demonstrated perfect dynamic flight stability of the aircraft while hovering.

Oktay and Kose [15] developed a model with a control system for a 4-rotor UAV. For the control system, a PID control algorithm was utilized as the controller for the UAV model and was tested by Matlab program simulations. Depending on the operational results of the Simulink models, the stationary PID controller gains for hover flight were 50, 5, and 50, for the longitudinal flight were 50, 5, and 50, and for the lateral flight were 100, 100, and 15, respectively. The developed controller successfully controlled the noise of the UAV dynamic models. During the flight operations, the rise time, overshoot, settling time, and steady-state error were within the acceptable limits of the design stability; and were between the boundaries of stability and critical flight situations.

Nguyen *et al.* [16] reviewed different control systems and algorithms of different types of UAVs (quadrotor, fixed-wing, rotary-wing, and hybrid wing-VTOL). Their objective was also to reduce the influence of external disturbances to enhance the quadrotor UAVs performance, such as reducing aerial collisions. This study provided an overview of the advantages and disadvantages of the controller systems, proposed optimal controllers, and UAV motor parameters to optimize future flight performance. In 2020, Chen and Jia [17] proposed a new linear controller for UAV hovering performance through an optimal control system consisting of a robust servo

linear quadratic regulator (RSLQR) and extended state observer (ESO). This system is similar to the PID controller but it showed better performance than the PID control, maintained hovering equilibrium to give the necessary stability for direct overhead hovering, controlling both UAV altitude and attitude. Additionally, the new controller was easy to implement in engineering systems and has a low cost. The new controller also has high overload resistance and strong anti-jamming capability.

If UAV aircraft operation is applied to agricultural fields, e.g., agriculture sprayer drone, there is an added payload to the aircraft takeoff. Aside from the spray equipment, there is also a spray fluid of approximately 30 kg (66 lbs) in total, or more, depending on the design of the spray fluid reservoir. This could greatly affect the aircraft's stability while performing the spraying operation, so it warrants special attention. Therefore, in agriculture, in order to perfectly manage spraying operations using UAVs, it is important to have a typical UAV's control system. From previous notes of my applied projects studies, and some of the previous studies on the use of UAV aircraft in agriculture applications, the longitudinal dynamic positions of the UAV aircraft have been linearized for the design of control systems for UAV aircraft. Depending on the presumed crop farming fields environments, longitudinal flight dynamics were proposed for flight data, including flying at speeds up to 90 km/h on average, or as hovering (stable slow flight) at lower speeds, and the aircraft actually hovering at altitude of approximately 60 m or a few meters [18-22]. So, the control designs (PID or LQR controller) are essential to adapt one or more sudden transient and unexpected accelerations of either all of the drone or variations of propellers poles to revolving shafts in the aircraft propulsion system. In addition to having such things in the UAV aircraft system as a compass, an accelerometer, a gyro, and a GPS, the availability of adequate powerful motors with a PID control system are crucial to maintaining the stability of the aircraft

when hovering. In this study, three PID controller terms were examined (the motors' speed, pitch angle, and pitch rate), as well as the LQR controller. So, the main objective of this article is the design of the best possible PID and LQR controllers that will maintain the motors' speed, and pitch angle and rate at any reference value despite the occurrence of disturbances. The best choice for the operation of the control system would be either a PID or LQR controller developed to functions with less error which could adversely affect the performance of the aircraft control systems. Consequently, the flying coordinate axes and forces acting on the UAV aircraft should be analyzed with the objective of obtaining certain stability of the UAV aircraft. For the UAV modeling and simulations in this study, the best available example to describe the UAV aircraft's flying stability can be found in the basic Matlab software process [23]. Matlab was used to obtain all the plots of the automatic control system for either the UAV aircraft in flight or in the process of being readied for flight. In conclusion, the objectives of this article are potentially interesting to some academics, engineers, and students; therefore, the importance of the field of UAV flight in agriculture is likely to influence the path of future research in the field of UAV technology, control, and systems management, especially in agricultural applications.

2. Materials and Methods

2.1 A Mathematical Modeling of the UAV Aircraft Dynamic State Variables and Control Inputs

Block diagrams were used in this study to represent the control systems generally in use in aircraft flying simulations of this type. Also, a Matlab approach was determined to be the optimal method to obtain all of the plots of an aircraft dynamic system which are defined in state space and to design robust PID and LQR controllers for an aircraft UAV, with respect to their asymptotic values as shown in the symmetric practical matrixes. This article presents the control system design process of a UAV which defines an optimal

equilibrium point, controls the hovering flight actuator, to manage the aerodynamic forces that may affect the aircraft in hovering flight or other unexpected disturbance problems for the UAV. Flight simulation was carried out to evaluate design results with high reliability and verify the effectiveness of the proposed control system strategy.

In general, UAV aircraft mode control angles are denoted by three angles: angle of orientation (yaw, ψ), twist or tilt movement (roll, ϕ), and directional up or down (pitch, θ). The following variables matrixes of the state-space model are for the UAV aircraft in flight. For this control design, only the longitudinal dynamic will be investigated. The proposed UAV aircraft model state will be as shown in Eqs. (1)-(3) [21, 22, 24-26]:

$$\begin{bmatrix} \dot{V} \\ \dot{\alpha} \\ \dot{q} \\ \dot{\theta} \end{bmatrix} = \begin{bmatrix} -0.1470 & 11.0767 & 0.0841 & -9.8065 \\ -0.0316 & -7.1712 & 0.8281 & 0 \\ 0 & -37.3527 & -9.9628 & 0 \\ 0 & 0 & 1 & 0 \end{bmatrix} + \begin{bmatrix} 3 \cdot 10^{-3} & 0.06 \\ 10^{-5} & 10^{-4} \\ 0.98 & 0 \\ 0 & 0 \end{bmatrix} \mathbf{U} \quad (1)$$

$$\mathbf{Y} = \begin{bmatrix} 1 & 0 & 0 & 0 \\ 0 & 1 & 0 & 0 \\ 0 & 0 & 1 & 0 \\ 0 & 0 & 0 & 1 \end{bmatrix} \begin{bmatrix} V \\ \alpha \\ q \\ \theta \end{bmatrix} + \begin{bmatrix} 0 & 0 \\ 0 & 0 \\ 0 & 0 \\ 0 & 0 \end{bmatrix} \mathbf{U} \quad (2)$$

$$\mathbf{U} = \begin{bmatrix} \delta_e \text{ elevator (deg.)} \\ \delta_t \text{ thrust (N)} \end{bmatrix} \quad (3)$$

where the state variables, \mathbf{V} is the velocity of UAV (m/s), α is the angle of attack (deg.), q is the pitch angular velocity rate (deg/s), and θ is the pitch angle (deg.), \mathbf{U} is the longitudinal control input of the tilt angle of the UAV control vector (deg.), and if the α , q , and θ are equal to 0, then $\mathbf{Y} = \mathbf{V}$, is the desired UAV aircraft velocity (m/s).

2.2 Physical-Mechanical Systems and Equations

For the scales of the physical-mechanical systems, control, and technical capability of the UAV, the

control designers should consider the following indicators.

2.2.1 The Control Design/State Observer Design

For convenience and modern control, many times a control designer will assume that all the states of a particular system are available for feedback. This is done to simplify the algebraic evaluation of a system's response or to help determine the quality of tracking that the particular system requires. Even though this is an essential tool for simplification, not all states are available for feedback in most real-life applications. If this is the case, a state observer can be designed which will estimate the unavailable state variables.

In evaluating the UAV longitudinal dynamic model, it was noted that the system has two control inputs (elevation and thrust) and four output states (velocity, angle of attack, pitch rate, and pitch angle). The two outputs (velocity and pitch rate) can be measured. The issue would be quite simple if the state that is wanted to evaluate was one of the two outputs, but if it is not, therefore an observer is required to estimate the state under investigation. Because not all states are available for feedback, but some are, a minimum-order observer could be used. This might be a nice solution, but instead, a full-state observer was developed for this project. That way a comparison can be made between the available state feedback and the estimated counterparts.

2.2.2 The Control Design/Observer Derivation

The first step to designing an operable observer is to understand the concept and derivation of one. Therefore, a brief overview of the derivation of an observer is required to describe the principles behind the structure of the observer design of this project. Now, consider the plant defined by the algorithm form of longitudinal as referred in Eqs. (4) and (5), i.e., for a state-space dynamic model [12, 25, 27]:

$$\dot{x} = Ax + Bu \quad (4)$$

$$y = Cx + Du \quad (5)$$

where state observer vector \dot{x} , x is state vector of implicit model variables, u is input vector (control input) of the implicit model, y is output vector, \mathbf{A} is the system

vector, **B** is the input vector, **C** is the output coefficients matrix and **D** is the feedback coefficients matrix.

Additionally, u is the state-feedback control of the UAV that can minimize the cost function, based on the observed state vector x , as illustrated in earlier works by Houari *et al.* [27], Kok *et al.* [28], and Ahmed *et al.* [29]:

Control input represented in Eqs. (6) and (7):

$$u = -\mathbf{K}\tilde{x} \quad (6)$$

where:

$$\mathbf{K} = \mathbf{R}^{-1}\mathbf{B}^T\mathbf{P} \quad (7)$$

where, \tilde{x} represents the transformation of x matrix, i.e., the estimated state of observer state vector x , **K** is a linear vector of state feedback gain.

The mathematical model of an observer is the same as the plant, except that the observer includes an extra term that introduces an estimation error. This error is used to compensate for inaccuracies in the **A** and **B** matrices and the lack of initial error. The estimation error, or observation error, is the difference between the measured output and the estimated output. The initial error is the difference between the initial state and the initial estimated state. Thus, the mathematical model of the observer, state observer vector \hat{x} can be shown as a longitudinal hovering state-space model in Eq. (8) [29]:

$$\dot{\hat{x}} = \mathbf{A}\hat{x} + \mathbf{B}u + \mathbf{L}(y - \mathbf{C}\hat{x}) \quad (8)$$

where \hat{x} is the estimated state vector, **L** is absorber gain vector, and **C** is the estimated output vector. The canonical diagonal variables of **C** matrix are ones, and the superdiagonal elements are zeros.

Using the Matlab/Simulink to simulate the step response of the system (controllability of states of the system) as in the variables of the previous mathematical model equation, the results of the state space matrices (**A**, **B**, **C**, and **D**) provided the following results:

$$\mathbf{A} = \begin{bmatrix} -0.147 & 11.08 & 0.0841 & -9.806 \\ -0.0316 & -7.171 & 0.8281 & 0 \\ 0 & -37.35 & -9.963 & 0 \\ 0 & 0 & 1 & 0 \end{bmatrix} \quad (9)$$

$$\mathbf{B} = \begin{bmatrix} 0.03357 & 0.06 \\ 1e^{-05} & 0.0001 \\ 0.98 & 0 \\ 0 & 0 \end{bmatrix} \quad (10)$$

$$\mathbf{C} = \begin{bmatrix} 1 & 0 & 0 & 0 \\ 0 & 1 & 0 & 0 \\ 0 & 0 & 1 & 0 \\ 0 & 0 & 0 & 1 \end{bmatrix} \quad (11)$$

$$\mathbf{D} = \begin{bmatrix} 0 & 0 \\ 0 & 0 \\ 0 & 0 \\ 0 & 0 \end{bmatrix} \quad (12)$$

The inputs to the system are, y and the control input u . **L** is a matrix that is called the observer gain matrix. The observer gain matrix is a gain matrix used as a way to weight the correction term involving the difference between the measured output y and the estimated output **C**. This term continuously corrects the model output and improves the performance of the observer. Since the observer is based upon the error feedback, an error vector must be found as in Eq. (13) [29-31].

$$\dot{x} - \tilde{x} = (\mathbf{A} - \mathbf{LC})(\hat{x} - \tilde{x}) \quad (13)$$

where $e = (\hat{x} - \tilde{x})$, which is the difference between state observer vector \hat{x} and estimated state vector \tilde{x} , will be defined as the least error vector (column vector) e .

The \dot{e} , error state equation (error dynamics) will be proposed as shown in Eqs. (14) and (15):

$$e = \text{eig}(\mathbf{A} - \mathbf{LC}) \quad (14)$$

$$\dot{e} = (\mathbf{A} - \mathbf{LC})e \quad (15)$$

From the equations above, it can be seen that the dynamic behavior of the error vector is determined by the eigenvalues of the matrix **A-LC**. Therefore, if the eigenvalues are selected so that the error vector is asymptotically stable and is relatively fast, then any error will converge to the origin with adequate speed. A way to check this condition is to see if the plant is completely observable. If it is, then it is possible to choose any matrix **A** or **L** such that **A-LC** has arbitrarily chosen eigenvalues. In order to determine whether the system is observable or not, the rank order definition, i.e., as referred in Eq. (16), can be used to determine whether the system has full rank or not. So, if the plant system is

observable, then it has full rank [32, 33]:

$$\text{Rank}[C \ CA \ CA^2 \ \dots \ CA^{n-1}] = n \quad (16)$$

where n (an observability matrix) is the number of states of the observable plant.

Now that the system has been considered observable, it is necessary to design a block diagram to accurately describe the observer's managing equations.

2.2.3 The Control Design/Determination of \mathbf{L}

Now that the block diagram has been created and the plant has been checked for observability, it is time to determine the matrix \mathbf{L} . For many complex matrix operations, there is no technique or it is difficult to determine stability such as the \mathbf{L} matrix efficiently. Usually, it is desirable to determine several of these matrices, where simulations are then worked to determine which provides the best performance. Most of the time in practical cases, the choice of the observer gain matrix boils down to a compromise between speedy response and sensitivity to disturbances and noise that may cause an interruption of the settled and peaceful condition of the UAV's flight. The technique used chiefly in this project to determine the observer gain matrix \mathbf{L} , was the implementation of an existing Matlab function called *place* (*placement*). To use the *place* function, you must enter an \mathbf{A}^T (transpose of the plant's \mathbf{A} matrix; the inverse of \mathbf{A}), \mathbf{C}^T (transpose of the plant's \mathbf{C} matrix; the inverse of \mathbf{C}), and \mathbf{p} (a vector of the desired eigenvalues for the observer) matrix into Matlab in the following manner in Eq. (17):

$$\mathbf{L} = \text{place}(\mathbf{A}^T, \mathbf{C}^T, \mathbf{P}) \quad (17)$$

Once the user has entered the following matrices, Matlab will calculate the observer gain matrix. Already from the plant, the \mathbf{A} and \mathbf{C} matrices are known, so the only unknown is \mathbf{P} , which can be chosen by the user. Shown below is the determined \mathbf{P} matrix, accompanied by the Matlab calculated observer gain matrix \mathbf{L} . The resulting observer and controller gain matrices are given in Eqs. (18) and (19):

$$\mathbf{p} = [-10 \ -11 \ -12 \ -13] \quad (18)$$

$$\mathbf{L} = \begin{bmatrix} 9.8530 & -0.0316 & 0 & 0 \\ 11.0767 & 3.8288 & -37.3527 & 0 \\ 0.0841 & 0.8281 & 2.0372 & 1 \\ -9.8065 & 0 & 0 & 13 \end{bmatrix} \quad (19)$$

2.3 Observer Implementation

Finally, once the observer gain matrix has been determined and the next step is to integrate the observer into the system. The observer will be connected to the system in the feedback loop, enabling it to receive the UAV output for manipulation by way of error differentiation into the new estimated states. This was accomplished by creating a new output identity matrix, or \mathbf{C} matrix, for the plant. The two outputs were then overlaid onto a scope output and compared. The action of the observer with similar stability margins is intended to reduce the crossover frequency of the control system feedback.

2.4 Design of the UAV Aircraft Controllers

For this project, it was decided that three controllers were to be made to control the longitudinal dynamics of the UAV aircraft. One is to be a PID-based controller, while the other two are LQR controllers (one full state feedback, and LQR with observer).

2.4.1 PID Controller Design

A PID controller is a simple tool that has been used many times to control numerous systems and performance would be quick and reliable (Fig. 1). The most common controllers that are used today are considered to be using the concept of PID control. PID controllers are considered convenient because they only require the tuning and implementation of three tuned gains. This is not to oversimplify the PID controller, things such as filters and lead/lag structures may be needed to help shape the response of the system, but overall the PID controller lightens the load for control engineers. The three gains needed for a PID controller are the proportional gain \mathbf{K}_P , the integrative gain \mathbf{K}_I , and the derivative gain \mathbf{K}_D . Overall, \mathbf{K}_P will make the system faster by reducing the rise time but the system will have more overshoot, \mathbf{K}_D reduces overshoot and settling

time, while K_I will reduce the steady-state error but the system will have a slow response with an increase in settling time and overshoot. Sometimes not all three gains are used in the controller, in which case the controller would take on the form PI or PD, but most commonly, a PID controller utilizes all three

gains. Practically, the Matlab/Simulink feedback function has been applied to obtain the closed-loop transfer function perfectly and directly from the open-loop transfer function. The simple PID controller dynamic system is shown in the actual block diagram (Fig. 1).

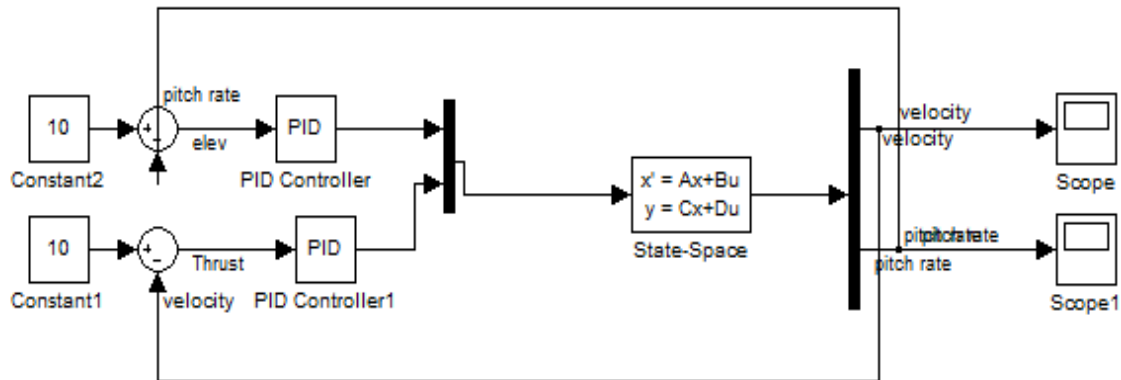


Fig. 1 A closed-loop system simulation diagram with a description of PID gain control of the UAV system.

The proportional gain is simply a multiplying factor, the higher you increase K_P , the higher or quicker your response will be to a step input. Increasing the proportional gain can improve the steady-state error, but it can also lead to higher overshoot.

The integral gain (K_I) looks at the error of the system. Increasing the integral gain reduces the area under the error curve, thus reducing and effectively eliminating the steady-state error in response to a step command. An integrator in the PID controller design will always multiply the integral gain.

The derivative gain (K_D) simply looks at the rate of the system response. Increasing the derivative gain will effectively increase the damping of the system. The reason for damping the system is to reduce oscillation as well as overshoot in response to a step command. The derivative gain will be multiplied by a derivative term in the PID controller.

2.4.2 Determination of PID Gains

Determining the values of the PID gains can be accomplished in a variety of ways, but for this project and this type of controller, the Ziegler-Nichols oscillation tuning method was chosen as shown in Table 1 as in Ziegler and Nichols [34]. This method

starts out with a pure proportional controller and the system is run with a step input. The initial value of the proportional gain starts small and is slowly increased or decreased until a stable oscillation begins to occur (oscillations with constant amplitude). The value of K_P at this point is called the ultimate gain K_{pu} . Once the ultimate gain has been determined, the critical period of the aircraft mode T_u , must be determined by means of Eqs. (20) and (21) [35]:

$$\omega = 2\pi f \quad (20)$$

$$T_u = 2\pi/\omega \quad (21)$$

where ω is the ultimate angular frequency at the ultimate period of aircraft mode T_u .

It can be found by finding the frequency of the oscillations created by the ultimate gain K_{pu} .

Once the ultimate frequency ω , and the ultimate gain K_{pu} have been found, then they can be plugged into the open-loop transfer function for the PID controller is shown in Eq. (22) as explained in Gao *et al.* [30, 31]:

$$H(s) = K_P (1 + (1/T_i s) + T_d s) \quad (22)$$

where K_P is the controller path gain, T_i is the controller's integrator time constant, and T_d is the controller's derivative time constant.

From the equation above, two equations can be

generated to solve for the derivative gain and the integral gain. These are shown below in Eqs. (23) and (24) as Ziegler-Nichols controller tuning [34]:

$$K_I = K_P/T_i = 0.5T_u \quad (23)$$

$$K_D = K_P T_d = 0.125T_u \quad (24)$$

Table 1 Ziegler and Nichols tuning table for system controllers [34].

Control type	K_P	T_i	T_d
P	$0.50K_{pu}$	∞	0
PI	$0.45K_{pu}$	$T_u/1.2$	0
PID	$0.60K_{pu}$	$T_u/2$	$T_u/1.2$

After all three gains were found, they were placed

into the system and run. This was done to confirm the gains calculated from the Ziegler-Nichols method. The PID control system is shown in the following figures with noise and without noise (Figs. 2 and 3). From these diagrams, it will be difficult to control the system with some noise without adding some implements to the control system. Observing from Figs. 2 and 3 that the waveforms of the responses were expected to be different, and by adjusting the value of K , the response may be unshot, overshoot, or undershoot with a continuous decrease in the amplitude of the response.

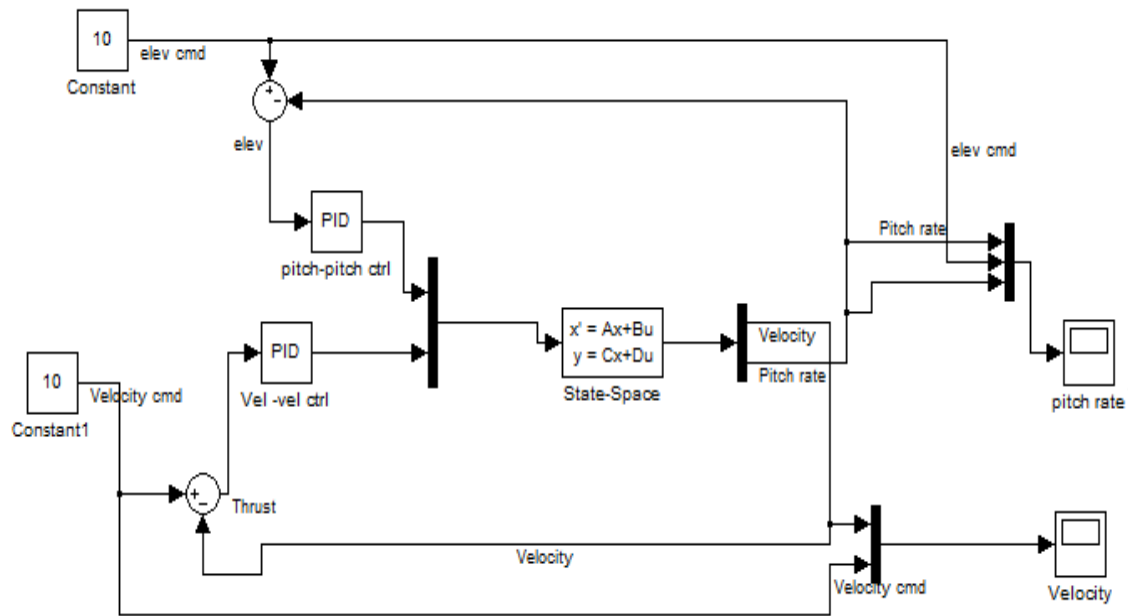


Fig. 2 Block diagram of the PID controller of UAV system without noises.

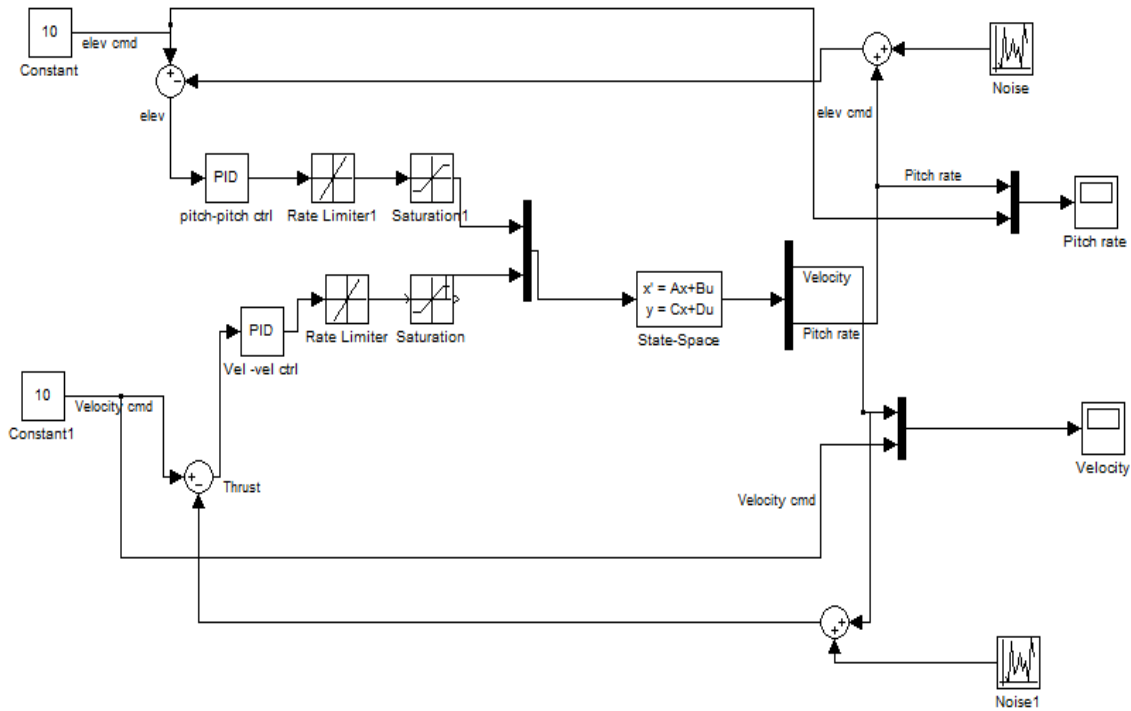


Fig. 3 Block diagram of the PID controller of UAV system with noises.

2.4.3 LQR Controller Design

Designing an LQR controller (optimal control) involves trying to optimize a controller (\mathbf{K}) to minimize the cost function on the state at any continuous-time t (0 to ∞) while also minimizing the time control input, and the performance index (J quadratic cost function) is as shown in Eq. (25) below [12, 21, 36]:

$$J = \int_0^{\infty} (x^T Q x + u^T R u) dt \quad (25)$$

where \mathbf{Q} and \mathbf{R} , are positive-definite Hermitian matrices or real symmetric matrices, x is the output response of the UAV's system to be reduced, and u is the control input.

The matrices \mathbf{Q} and \mathbf{R} determine the relative importance of the error and the expenditure of this energy. These matrices are chosen arbitrarily and are based on weighting issues. In order to determine if the dynamic system model is controllable or not, the rank order definition of Eq. (26) can be used to determine if the system has full rank or not. One condition placed on the \mathbf{Q} matrix is:

$$\text{Rank} [\mathbf{Q} \quad \mathbf{Q} \mathbf{A} \quad \mathbf{Q} \mathbf{A}^2 \quad \dots \quad \mathbf{Q} \mathbf{A}^{n-1}] = n \quad (26)$$

where n (a controllable matrix) is the number of original states in the plant model.

Besides minimizing the cost, the function of the LQR should be designed to track a step command. The principal behind a regulator problem is to drive the states to an equilibrium point. Now, to get zero steady-state error for the response to a step command, an integrator must be added to the system. When this integrator is added, it also adds another state to the system. This new state can be defined as an error state and the best way to get tracking is to regulate it. Therefore, if driving the error state to zero (an equilibrium point) is the desired goal, then an LQR controller is appropriate. Before diving off into designing an LQR controller, some assumptions must be made to drive the plant system to the desired state, and these assumptions to achieve the desirability of a stable plant system are as follows: because there is no feedback loop, the open-loop system function has a desirable integrator dynamic property of control system of the plant behavior, the system has a negative feedback control system (full state feedback), and state

feedback matrix $A-BK$ is stable, i.e., the eigenvalues of $(A-BK)$ have negative real parts or to deliver negative feedback.

The Q (square state) and R (unitary input) weighting or arbitrary matrices have been optimized in the cost function, and these matrices can be plugged into Eq. (27) (the Riccati Equation), from where P , the solution of Riccati equation, can be solved [17, 28]:

$$A^T P + PA - PBR^{-1} B^T P + Q = 0 \quad (27)$$

Now, P has been solved. It can be plugged into Eqs. (28) and (29), as referred in Chen and Jia [17] and Kok *et al.* [28]:

$$R = -BR^{-1} B^T \quad (28)$$

$$K = R^{-1} B^T P \quad (29)$$

For this project, Matlab was used to compute the K matrix. Using Matlab programming or by plugging the P matrix into the equation above, the gain matrix K of LQR control can be solved. There is a command in Matlab called LQR that calculates the gain matrix K , the P matrix, and the error vector E . The inputs to this command are the A and B matrices from the plant and the Q and R matrices that were chosen arbitrarily. The following mathematical approach Eq. (30) shows how this command is used to find K or P values [12].

$$[K, P, E] = \text{lqr}(A, B, Q, R) \quad (30)$$

The final design values of the LQR controller are as follows in Eqs. (31) and (32):

$$R = \begin{bmatrix} 1 & 0 \\ 0 & 1 \\ 0 & 0 \\ 0 & 0 \end{bmatrix} \quad (31)$$

$$Q = \begin{bmatrix} 2 & 0 & 0 & 0 \\ 0 & 2 & 0 & 0 \\ 0 & 0 & 2 & 0 \\ 0 & 0 & 0 & 2 \end{bmatrix} \quad (32)$$

Also, the gain matrix sets the open-loop poles to the desired locations and establishes the decoupling eigenvector structure.

By using the previous K equation or also using the Matlab programming, K values can be determined.

This yields the state feedback gain vector which will be as given in Eq. (33), i.e., optimal gain matrix K of LQR control.

$$K = \begin{bmatrix} -0.8938 & -7.3439 & 1.2880 & 18.7708 \\ 0.1440 & 0.4591 & -0.0604 & -1.0876 \end{bmatrix} \quad (33)$$

Therefore, the values of K and P , which could be determined mathematically, can be used to minimize the cost function. When you need to minimize the cost function, the values of K or P can be reduced, which means you need to pick small values of P or K . The LQR controller designs are shown in the following diagrams (Figs. 4-6).

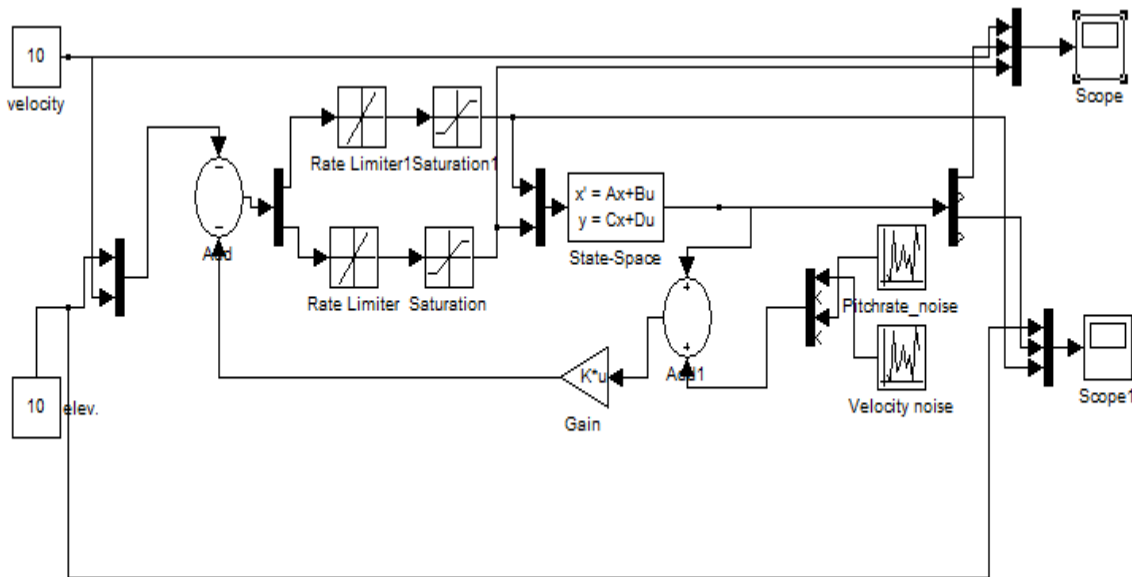


Fig. 4 LQR controller block diagram without an observer.

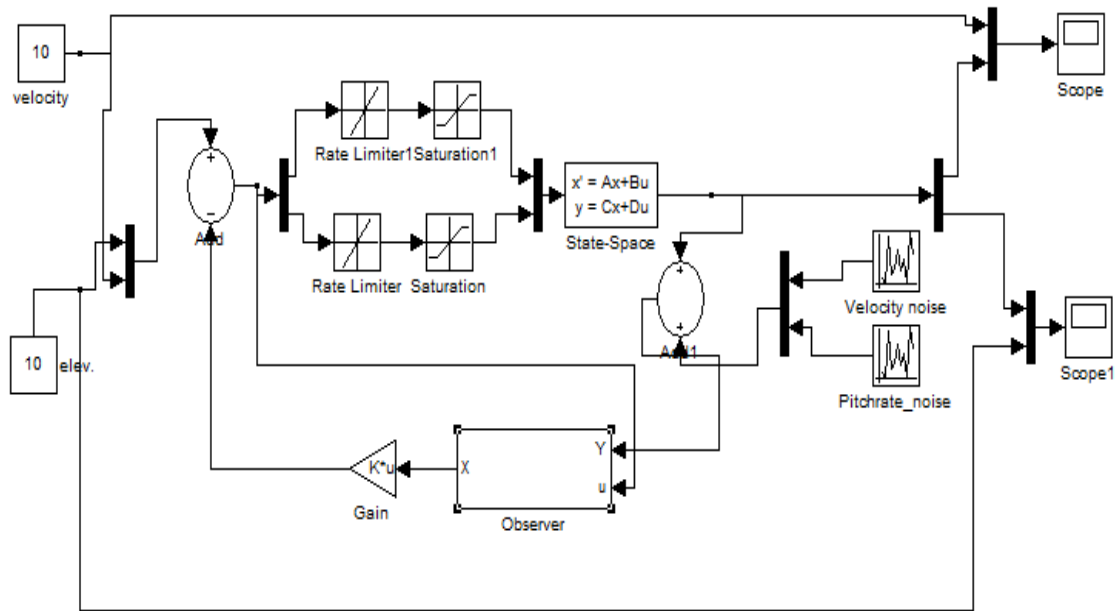


Fig. 5 LQR controller block diagram with an observer.

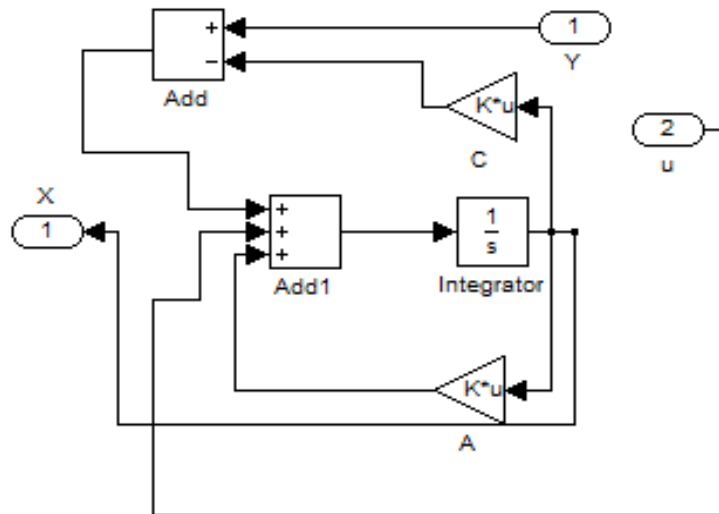


Fig. 6 Schematic diagram of the observer design (for LQR control).

3. Simulation Results and Discussion

3.1 Sensitivity and Complimentary Sensitivity: A Good Tracking

The PID and LQR controllers were designed to ensure that the UAV aircraft is stable within certain limits and reference conditions. The controllers should be able to track the reference variables for the UAV flight tracking system while another observer-LQR controller was regulating the amplitude and attitude.

When evaluating the tracking ability of a controller, one must remember that to achieve perfect tracking, the number of control inputs must be greater than or equal to the number of performance outputs. In addition, there will be exterior sources added into almost every practical system, such sources include noise and disturbances. These effects can sometimes have a profound effect on the controller's tracking ability. However, two concepts are available to help relate these external sources to the tracking of the system:

sensitivity and complementary sensitivity. Sensitivity relates a change in closed-loop tracking to a change in the open-loop plant. The definition of tracking is that the output should follow a reference command, or the output y should equal the input r and the error e should be equal to zero as shown in the simple diagram below (Fig. 7).

The solving of the three transfer functions of the system will be as a function from the reference input r to the output y , as referred in Eq. (34) [37]:

$$y = \frac{PK}{1 + PK}r + \frac{P}{1 + PK}d \quad (34)$$

A tracking controller can be used in place to improve the tracking error of the output, $e = (r - y)$.

$$e = \frac{1}{1 + PK}r - \frac{P}{1 + PK}d \quad (35)$$

$$\delta = \frac{K}{1 + PK}r - \frac{PK}{1 + PK}d \quad (36)$$

Also, transfer functions can be joined into one as pointed in Eq. (37), where r is a reference input, d is a disturbance, and n is a measurement of noise:

$$y = \frac{PK}{1 + PK}r + \frac{P}{1 + PK}d - \frac{PK}{1 + PK}n \quad (37)$$

Thus, the values of S and T will be calculated as represented in Eqs. (38) and (39):

$$S = \frac{1}{1 + PK} \quad (38)$$

$$T = \frac{PK}{1 + PK} \quad (39)$$

where S is the sensitivity and T is the complementary sensitivity. By using S and T in the equation above (i.e., y equation), the following new equation can be written as in Eq. (40):

$$y = Tr + SPd - Tn \quad (40)$$

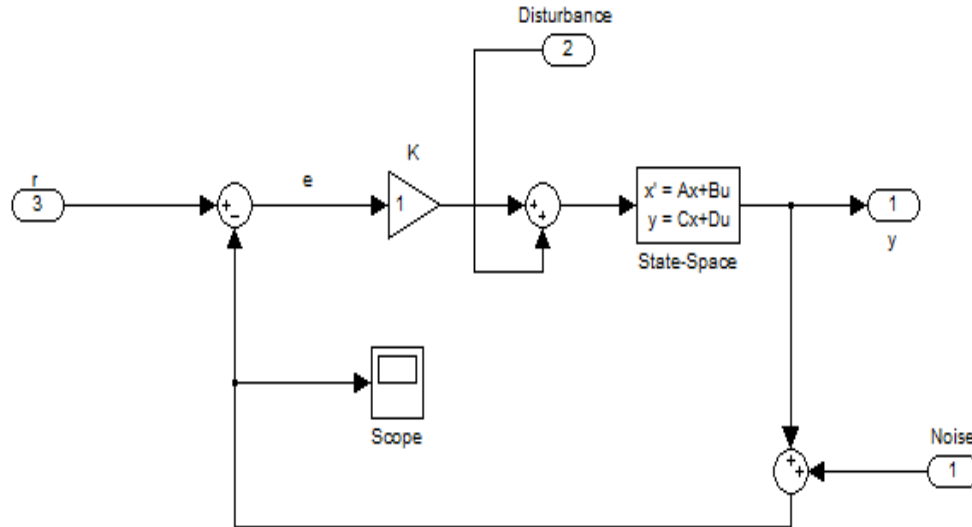


Fig. 7 Closed-loop block diagram of the effect of noise and disturbance on the control system.

From $S + T = 1$, the final equation for this system will be as notated in Eq. (41):

$$\frac{1}{1 + PK} + \frac{PK}{1 + PK} = \frac{1 + PK}{1 + PK} = 1 \quad (41)$$

From this equation, you can now determine the steps needed to enhance the loop gain, PK , to help with tracking and noise reduction.

3.2 Controller Performance

All three controllers have been designed and implemented into the UAV system. The next step is to evaluate their performance and robustness. These controllers should meet the required specifications, while still being stable and robust.

The robustness of this system is measured by the phase/gain margins and bandwidth. The phase and gain margins are metrics of the robustness with respect to gain/phase errors in the loop gain. The gain margin, a

measure of relative stability, is defined as the magnitude of the reciprocal of the open-loop transfer function, evaluated at the frequency at which the phase angle is -180 degrees. It can be shown by the following notation in Eq. (42) [38]:

$$GM \equiv \frac{1}{|GH(\omega_\pi)|} \quad (42)$$

where $GH(\omega_\pi) = -180^\circ = -\pi$ radians, and ω_π is the phase crossover frequency, and GM is the gain margin.

The phase margin (PM), a measure of relative stability as well, is defined as 180 degrees plus the phase angle of the open-loop transfer function at unity gain. The formula for PM can be shown as follows:

$$\phi_{PM} = [\arg GH(\omega_i) - (-180^\circ)] \text{ in degree} \quad (43)$$

where $\arg GH(\omega_i) = 1$ (the phase lag), and ω_i is the gain crossover frequency.

3.3 Stability Analysis by Using a Bode Diagram

A bode response diagram is another stability analysis method that can be used to give a particular assessment of the PM and gain margin to determine an exact stability state in the deployed control system. The following bode plot figures (Figs. 8-10) show the frequency characteristics of the system function: the PM, GM, and bandwidth for the UAV control system. Effect of the UAV controller from thrust to pitch rate resulted in an equivalent crossover frequency of 8 rad/s with an 85 dB gain margin and 180 deg. phase margin (phase margin = inf. deg. at inf. rad/s) as shown in Fig. 8, but the visible phase difference only represents a 450 deg. phase shift. Also from the figures, gain and PMs are undefined (infinite), because there is no crossover at 0 dB and there is no crossover at -180 deg. Furthermore, the first bode plot has a phase of 270 degrees at a frequency of 1 rad/s (Fig. 8), the second bode plot has a phase of 0 degrees at a frequency of 1

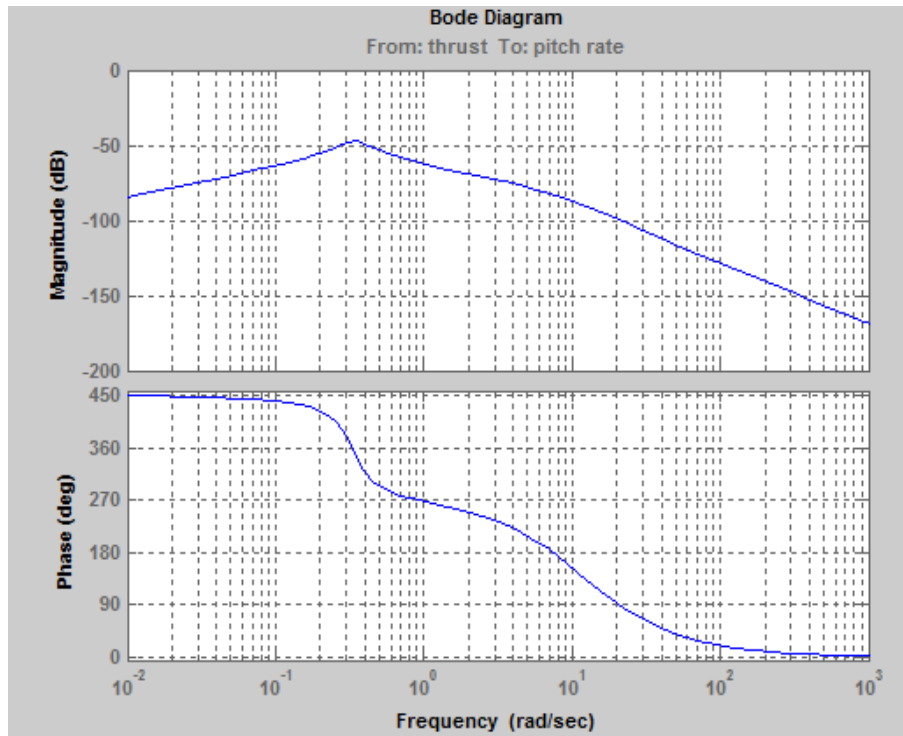


Fig. 8 Bode diagram of UAV controller from thrust to pitch rate.

Functional Sustainability of a Flight Dynamics Control System for Stable Hovering Flight of an Unmanned Aerial Vehicle (UAV), such as in Agricultural Applications: Mathematical Modeling and Simulation

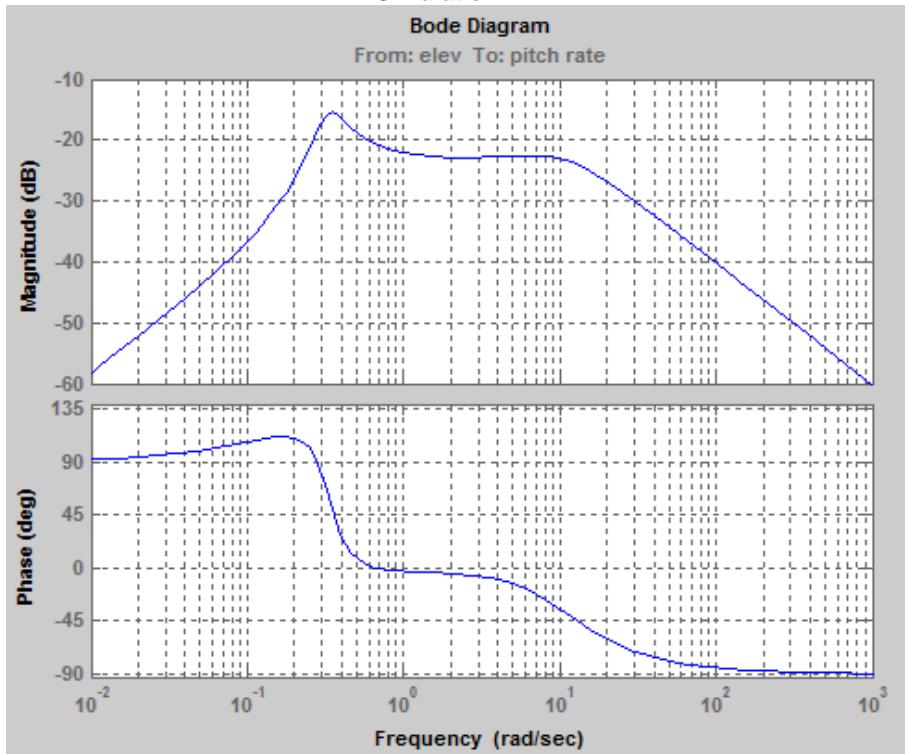


Fig. 9 Bode diagram of UAV controller from the elevator to pitch rate.

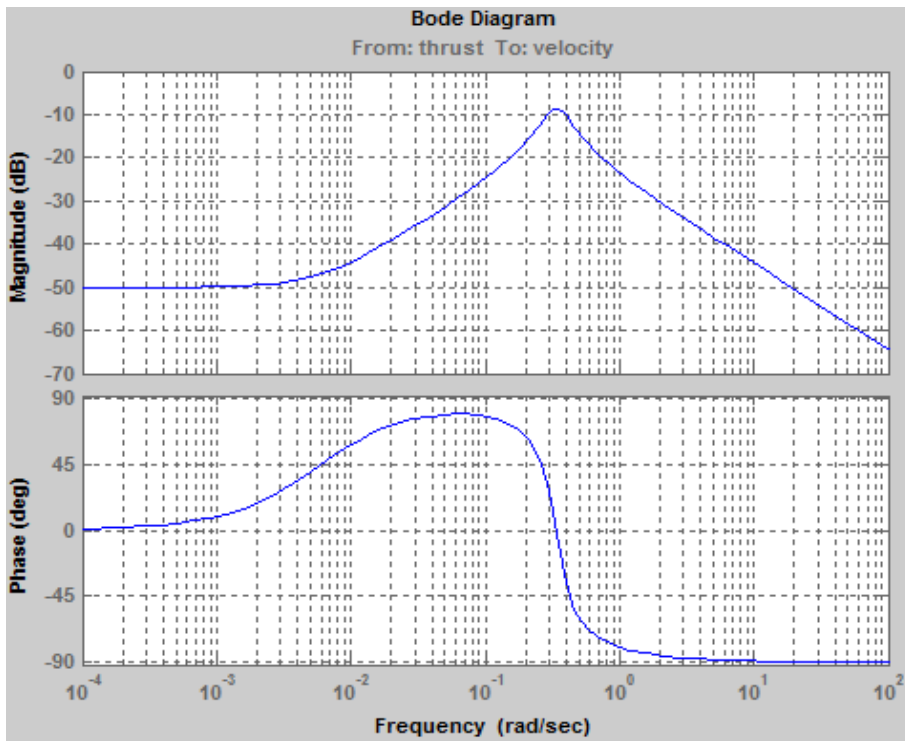


Fig. 10 Bode diagram of UAV controller from thrust to velocity.

rad/s (Fig. 9), and the third bode plot has a phase of -78.75 degrees at a frequency of 1 rad/s (Fig. 10).

Clearly, the PM for the response is infinity, whereas the gain margin is approximately 85 dB and the gain cross-

over frequency is 8 rad/s. The system is quite stable because the gain margin is greater than 0 dB and the phase margin (infinite) is greater than 180 deg. So, the system will be stable for whatever disturbance it may encounter, and the figures show other margins for the response as infinity, so again, the system will be stable for whatever disturbance it may encounter.

Generally, results from Fig. 11 show a gain margin (dB): amplitude ratio below 0 dB when phase angle = -180 deg.; phase margin (deg.): phase angle above -180 deg. when amplitude ratio = 0 dB; and gain and phase margins can be used for measuring the plant system stability. High-frequency response is well predicted by the proposed model. The effect of the UAV controller from the elevator to velocity resulted in an equivalent crossover frequency of 0.88 rad/s with 0 deg. phase margin and within 0 dB gain margin. So at this frequency, the phase is 0 deg., thus the phase margin is 180 deg. the gain margin is undefined (infinite) since there is no crossover at -180 deg. phase margin.

Unfortunately, the amplitude margin only has 180 deg. of phase margin at 0 dB, so response will be underdamped at that frequency of minimum phase margin at 0.88 rad/s. The positive and high levels of both gain margin and phase margin indicated plant system stability. Fig. 11 below also shows that the system could be in the marginally stable system range with both the phase and gain margins all being zero (phase margin being equal to the gain margin or $\omega_{pc} \geq \omega_{gc}$). Evidently, the gain margin for the response is infinity, whereas the phase margin is at 180 deg. and gain cross-over frequency is 0.88 rad/s. The system is quite stable because the gain margin is greater than 0 dB (infinite) and the phase margin is greater than 90 deg. Finally, the system could be stable for whatever disturbance it may encounter at any instant. Thus, the UAV aircraft system condition is absolutely perfect, in that even if it encounters a disturbance, the system is able to maintain its stability and operate as intended.

From the simulation result shown in Fig. 12 below,

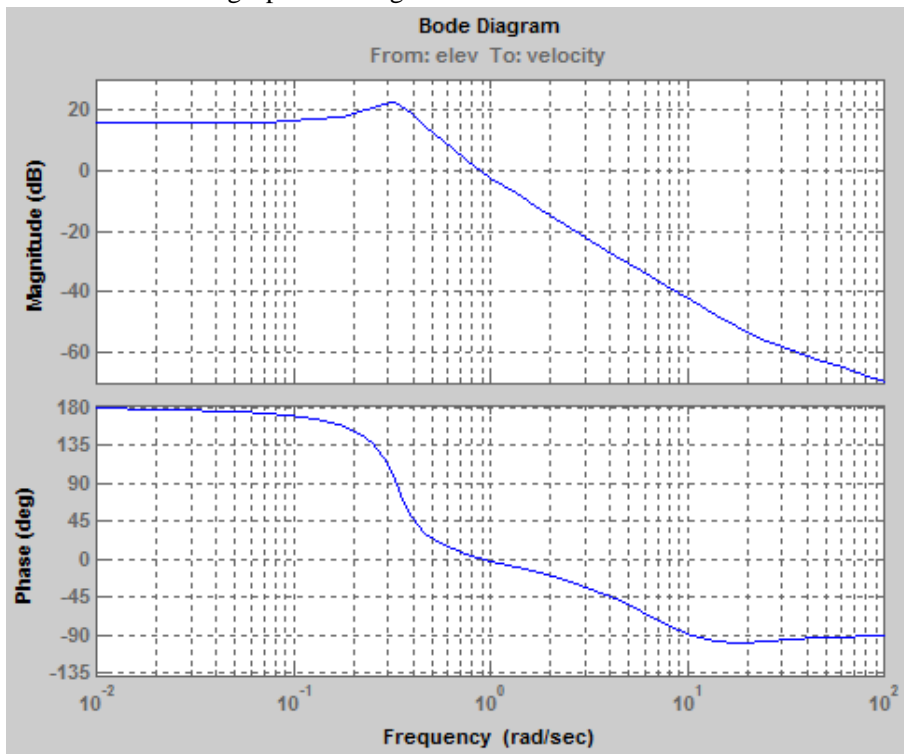


Fig. 11 Bode diagram of UAV controller from the elevator to velocity.

any input command of all commands of UAV states controller sufficiently decreases any disturbance to the

velocity and pitch rate making them correspond to the performance capabilities. Rapid response of the UAV

system indicates flight stability by reducing both rise time and settling time. The linear velocity (m/s) and pitch rate (deg/s) in the initial mode, show a very light-ripple with time (in seconds), which causes the aircraft to oscillate at a low frequency for a short period then the oscillations disappear and return to the reference state. This behavior is the intentional result of the all-UAV state controller. Although the linear velocity response may contain an unacceptable error rate, the same thing does not occur as indicated by the pitch rate transfer function result, thus the system reaches the steady-state condition in 42 s from its initial condition. Moreover, this system has oscillations occurring from 0 to 42 s with clear overshoot, but the system is still in a stable condition. Also, Fig. 12 depicts that there are only very small oscillations at almost 40 s, the overshoot decreases to almost -1.45 m/s at time 4 s, and settling time becomes too short around 42 s which satisfies the required parameters up to hovering conditions. Through the use of an all UAV controller,

the performance characteristics of aircraft system parameters are drastically improved, yielding perfect proficiency in hover stability.

3.4 Stability Analysis by Using Root Locus

The plot of this system has two real zeros and a pair of complex poles. The open-loop system poles are 0 and -1, controlling gains of the aircraft system make the plant poles meet the desired specification positions, which means with the controller gains, the state of the poles, can be moved significantly to gain a proper overshoot and desired settling time. For the stability of the controller systems, the pole/zero plots will be given to show the placement of the poles. Poles of a system would affect the time response of the system. So, the simulation results are shown as the pole/zero plot locations for the UAV controller (Figs. 13-15).

In the beginning, in Fig. 13, as shown by the plot, the control system specifications were not fully met due to zero value (-7). A negative zero (o—o), which is

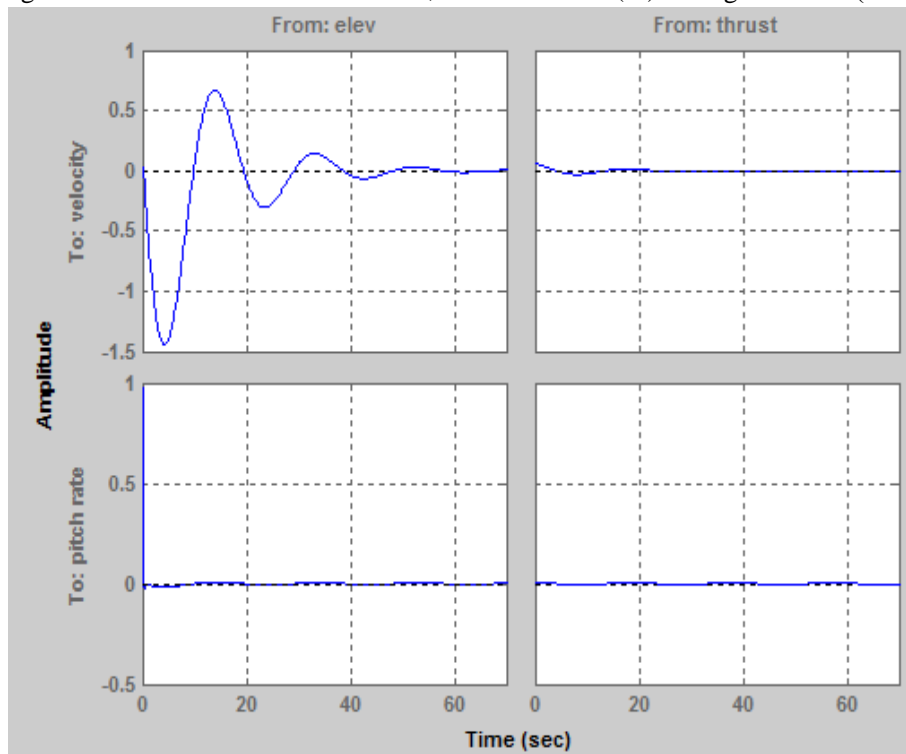


Fig. 12 Bode plot of all UAV states controller.

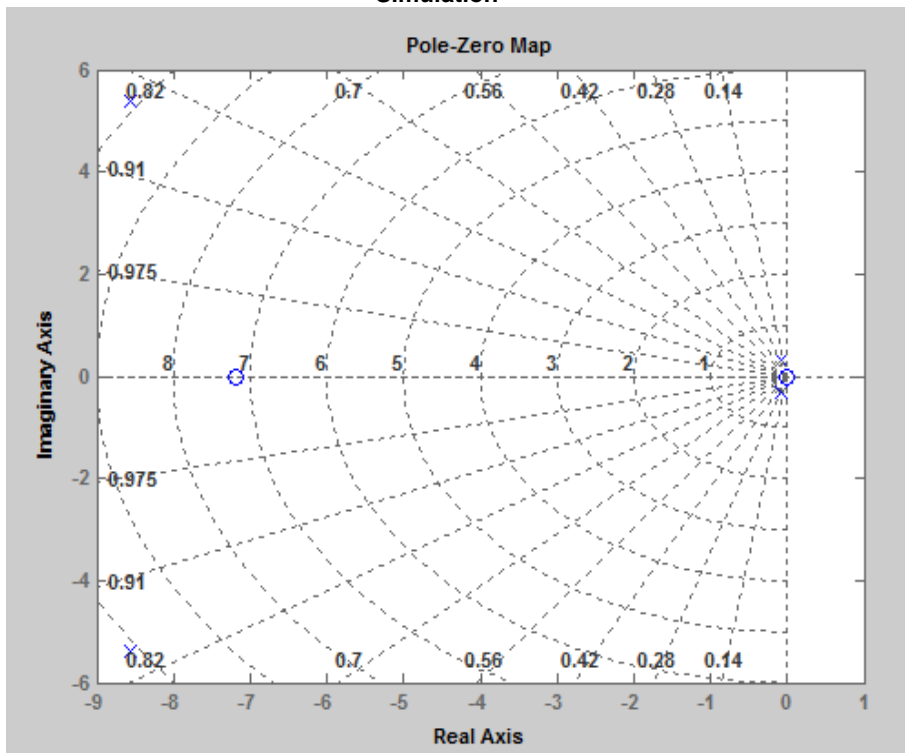


Fig. 13 Root locus (poles and zeros) map for the UAV control system.

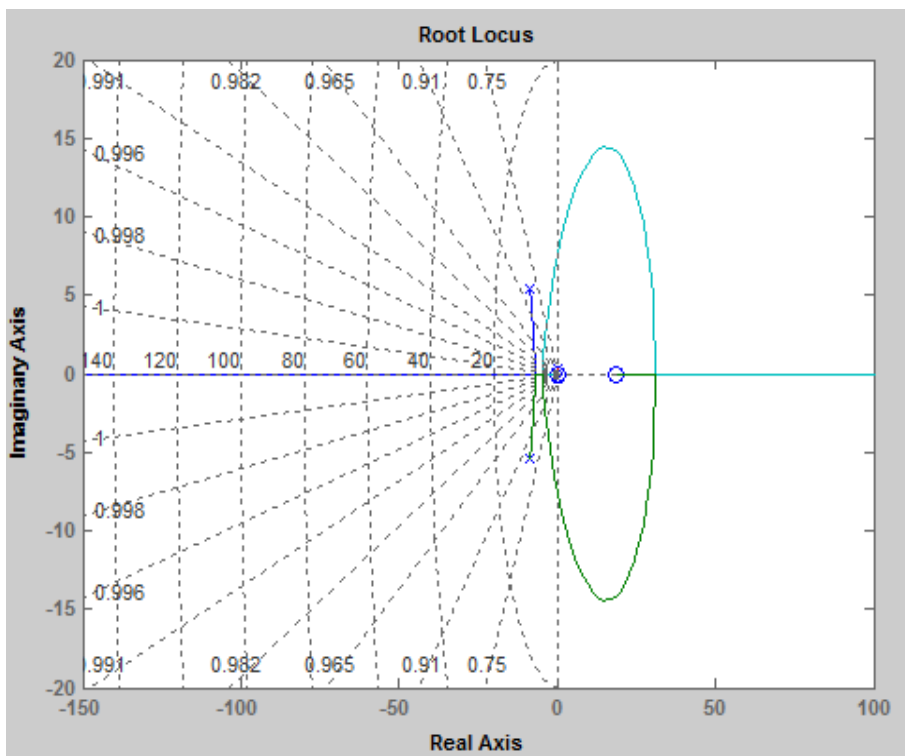


Fig. 14 Methodology plot of root locus for UAV controller analysis.

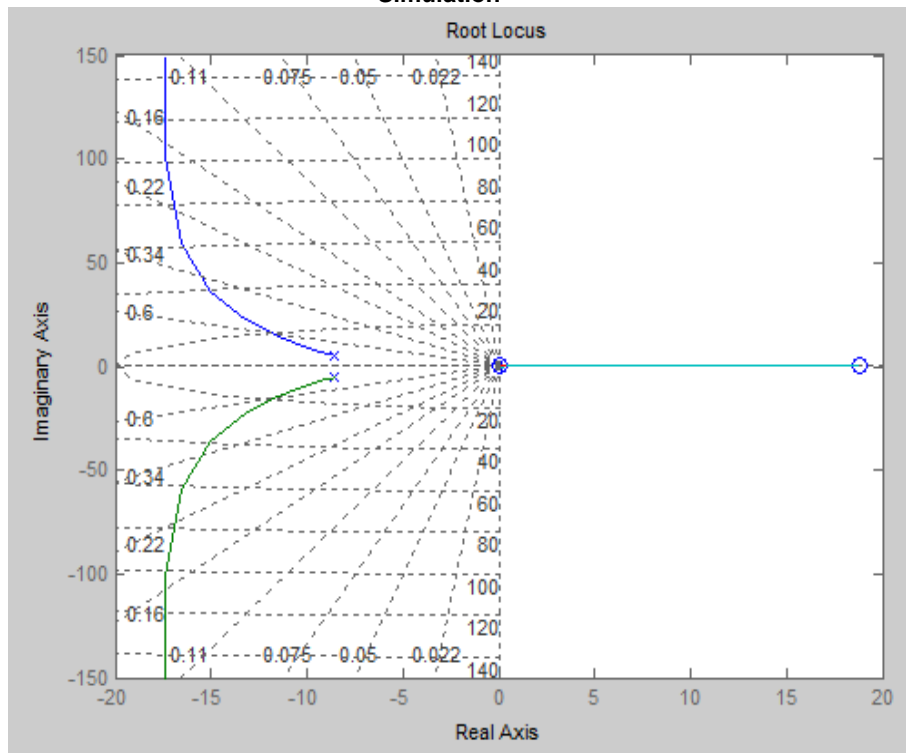


Fig. 15 Root locus (poles and zeros) stability maps for the UAV control system.

located on the real axis, is equivalent to the system response requirement by adding a proper response of the system and tuning the controller gains to get the required response values. So, the overshoot, in this case, may be greater than the required overshoot. However, since the zero is slightly larger in magnitude (≈ -7), its effect decays very quickly. Therefore, this is an underdamped system in which there is a pole pair and it also has a restricted zero pair (0 and ≈ -7). So, it is evident when the root locus diagram analyzes that there is a clear pole pair (\times — \times) in the left half of the s -plane and the pole/zero both have an equal number (≈ 6 and ≈ -6) (Fig. 14). The controller system of the UAV is stable when all-pole pairs lie in the left half of the s -plane and the system poles have met the desired specifications that would also achieve good stability based on having less settling time and less peak time. Therefore, the results of Figs. 14 and 15 demonstrate the stability of the current aircraft system. The primary impact is on the short-period roots, so delaying time may modify the asymptotes of the root locus. Also, the

system is becoming stable when the pole/zero system plot goes to the right of the single point $(-1, 0)$, and the gain margin is positive in dB.

3.5 Stability Analysis by Using Controller Response

Analyzing the UAV aircraft dynamic system time-response behavior for hovering stability, Figs. 16 and 17 below show the PID controller response displayed as the linear velocity (m/s) versus time in seconds. Although this system contains some disturbance noises, it gave acceptable results with reduced rise time and steady-state error along with increasing negative overshoot and a small decrease in settling time. Although the UAV system is stable, its initial response to the input variables shows obvious oscillations, settling time, extensive overshoot, and a clear steady-state error (T_r rise time = 10.7 s, T_s settling time = 54 s, T_p peak time = 4.35 s with maximum overshoot -62.2 m/s), and the maximum peak value of the velocity response (maximum overshoot) was initially in negative gradient descent. Fig. 17 below shows that this

UAV aircraft takes a relatively long time, about 70 s, to settle to its equilibrium state when given velocity disturbance noises. On the other hand, Fig. 16 below illustrates that the UAV aircraft may oscillate at a high rate when launched, but it returns to a stable state in a short period of time due to the control system. Also, the PID controller response of velocity (m/s) with time in seconds without noise was significantly precise overall. The main aim of the controller system is to reduce the disturbance effect to an insignificant level. It can be seen from Fig. 16 the PID controller response on the UAV aircraft velocity (m/s), where reduced rise time (0.22 s), T_s settling time = 9 s, T_p 0.44 s overshoot time with peak velocity amplitude 8.85 (m/s), and clear steady-state error. Now, with the PID controller, the system could achieve a stable linear velocity (m/s) without an excessive overshoot, with rapid rise time, and velocity error in the range of ± 10 (m/s). The overall control system of the UAV aircraft (response of the velocity in m/s) responds very quickly and is almost stable in less

than 9 s with no consistent steady-state error, thus the aircraft response seems to be reasonable. Also, although this aircraft takes a somewhat long time to settle to its equilibrium state when given a velocity disturbance noise, the UAV aircraft system has the ability to return to its equilibrium after disturbance in less than 54 s.

Figs. 18 and 19 below show the PID controller response of the pitch rate (deg/s) with time in seconds. Although this system contains some disturbance noises, it gave acceptable results as it reduced both the rise time and the steady-state error with increasing negative overshoot and decreased the settling time a small amount. Although the UAV system is stable, its initial response to the input variables shows obvious oscillations, settling time, extensive overshoot, and clear steady-state error (T_r rise time = 9 s, T_s settling time = 54 s, T_p peak time = 4.7 s with peak pitch rate amplitude -5,714 deg/s) where the amplitude of the pitch rate was initially in a negative gradient descent (Fig. 19). Fig. 19 shows that this UAV aircraft takes a

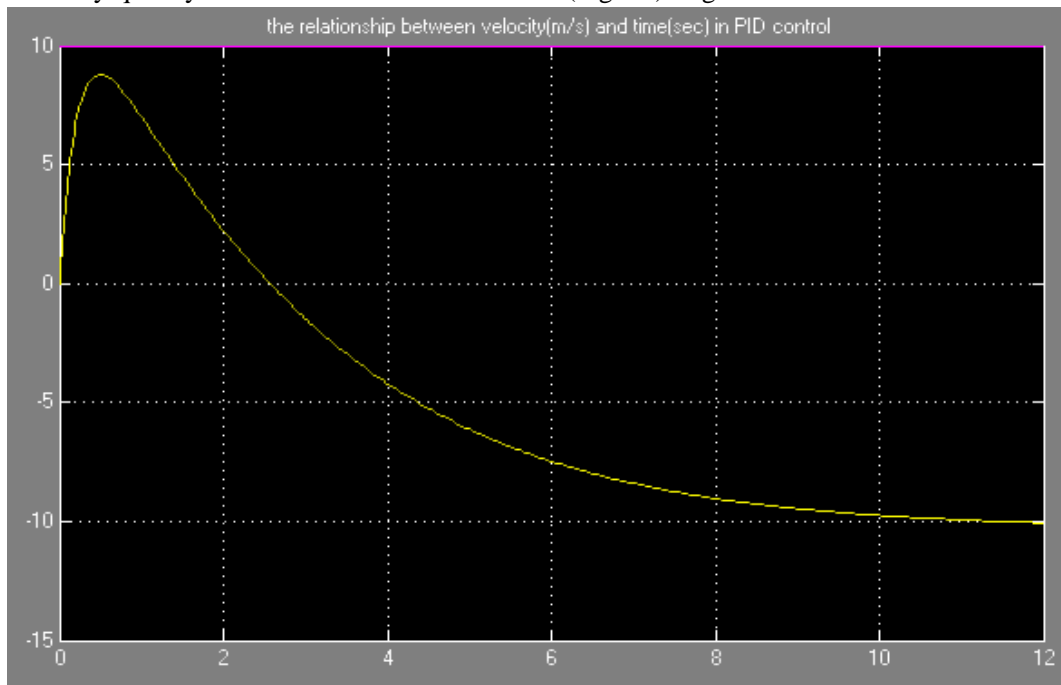


Fig. 16 The relationship between velocity (m/s) y-axis and time (s) x-axis in PID control without noises (response of the control system).

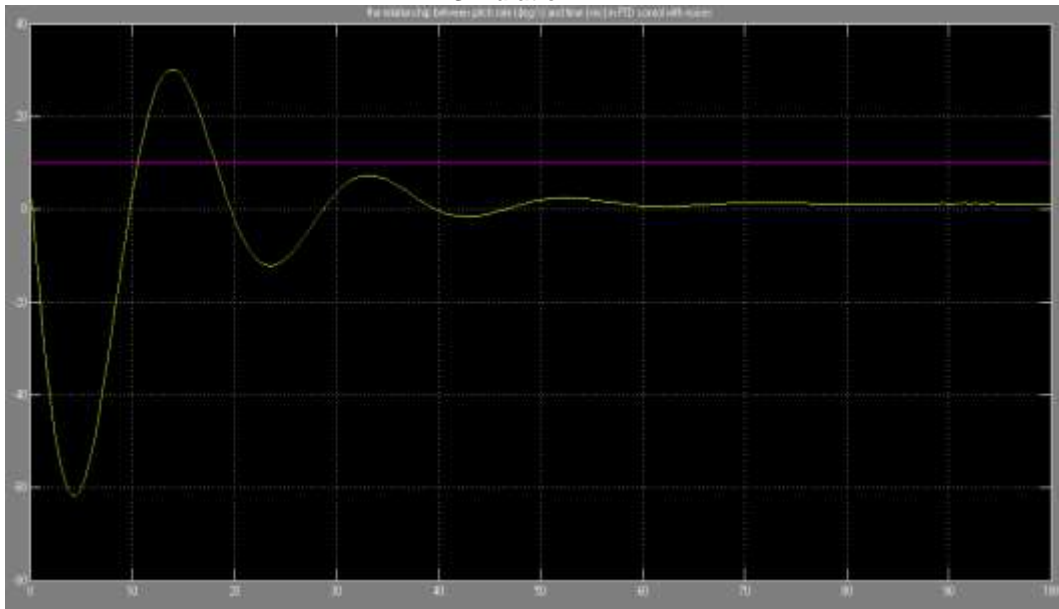


Fig. 17 The relationship between velocity (m/s) y-axis and time (s) x-axis in PID control with noises (response of the control system).

somewhat long time to settle to its equilibrium state when given a pitch disturbance noise. It takes about 70 s to reach a steady state. On the other hand, it can be noted from Fig. 18 that PID controller response of pitch rate (deg/s) with time in seconds without noises was significantly precise overall with about 10 as the final output value to a unit step input. It can be seen from Fig. 18, the results of the PID controller response on the pitch rate (deg/s), reduced the rise time (0.22 s), T_s settling time = 9 s, 0 overshoot, and almost eliminated the steady-state error. Now, with the PID controller, the system could achieve a pitch rate (deg/s) without overshoot, with rapid rise time, and almost no steady-state error or at least very close to zero, which means that the system response shows that the controller eliminated the steady-state error. The overall control system of the UAV aircraft (response of the pitch rate in deg/s) responds very quickly and is almost all the way to stability in less than 9 s with no consistent steady-state error; thus the overall aircraft response seems to be reasonable. In addition, although the aircraft system simulation takes a somewhat long time to settle to its equilibrium state when given a disturbance noise in pitch rate, the UAV aircraft system has the ability to return to its previous steady motion in less than 54 s after

disturbance which means the disturbance effect is reduced to a trivial level. Also, in normal reality, a prolonged period of stability may be affected by a change in pitch rate as a result of an unexpected weather incident or some instability in the pitch angle.

Practically, Figs. 18 and 19 illustrate the pitch rate (deg/s) of the PID control without and with noises, where the response of the control system without noises is ranged between 0 and +10, which meets the acceptable system requirement. Also, the pitch rate response does not show any overshooting value and clearly no steady-state error, and importantly, the linear velocity response in the PID control system shows somewhat better performance than pitch rate in the same time intervals (Fig. 16). Figs. 16 and 18 show that the pitch rate (deg/s) and linear velocity (m/s) of the PID control without noises are in the range of ± 10 , which meets the acceptable system requirement. In addition, there is a close correspondence of the response of the PID control with noise disturbance expressed in velocity (m/s) and the pitch rate (deg/s), i.e., settling time = 54 s, as shown in Figs. 17 and 19. However, the variance between the linear velocity (m/s) and pitch rate (deg/s) is clearly visible based upon the effect of the PID controller without disturbance noises.

Although there are close similarities between the two variables, a steady-state error exists, which means the PID controller may not be capable of eliminating the steady-state error. Although the response of the linear velocity and pitch rate transfer function results with noises may contain unacceptable error rates, the system reaches the steady-state condition in 54 s after disturbance from its initial condition. Moreover, this system has oscillations from 0 to 54 s with clear overshoot, but the system with the PID controller is still in a stable condition. Even in the case of overshoot, the model is acceptable for all system steady-state, even when influenced by disturbance (noise).

Generally, a perfect PID controller system would efficiently affect the three parameters (three angles) of the aircraft orientation, i.e., angular coordinates of the UAV platform, which are: pitch θ , roll ϕ , and yaw ψ . So, to achieve UAV aircraft stability, the PID coefficients (P, I, and D) values should be set to proper values for each aircraft orientation (pitch θ , roll ϕ , and yaw ψ) of each individual design model. The complete stability system should contain a PID controller for each one of the aircraft pitch, roll, and yaw variables; as well as for the entire UAV aircraft, as a change in any of these parameters can cause turbulent and oscillatory behavior of the flight system. Thus, any variation of controller coefficients (gains) in any of the controllers shifts the effectiveness of the UAV stabilization. To achieve UAV stability, appropriate controller coefficient settings should reduce the rise time, reduce the settling time, and eliminate the steady-state error. With proper controller configurations, the stabilization state of the UAV aircraft can be achieved

by any PID and LQR control system with linkages connecting the aircraft to its dynamic parts and allowing the relative motion between those dynamic systems to bring the aircraft to proper stability regardless of flight conditions.

The flight mode simulation results are shown in Figs. 20 and 21. These figures show the parameters of overshooting and its relationship with the system feedback gain. The feedback gains of the control system depend on the system steady-state and the stability parameters. Maximal value of the feedback gain, which appears between the system parameters, increases corresponding to the ratio between the steady-state levels of all system parameters (blue line vs. other color lines). The LQR design state includes linear velocity (V), angle of attack (α), pitch rate (q), and the pitch angle (θ) that are required for the stable response of system output which can be achieved by using the LQR controller that meets the dynamic design variables for the UAV aircraft. In addition, the figures below show the system response of the UAV aircraft pitch rate (deg/s) and linear velocity (m/s) for time samples vector (in second) and the simulated time response of the dynamic system to arbitrary input parameters which were quite coded in different colors. Fig. 20 shows that the variable of the LQR controller (red line) produces a smaller control input in the initial response, which avoids the incident of massive angle rates. The LQR control shows a higher overload resistance capability and better performance than the PID control (blue line) with a 0% peak overshoot percentage, whereas the LQR controller is indicating a faster response. Thus, all specification inputs of the dynamic system are convinced and satisfied.

Functional Sustainability of a Flight Dynamics Control System for Stable Hovering Flight of an Unmanned Aerial Vehicle (UAV), such as in Agricultural Applications: Mathematical Modeling and Simulation

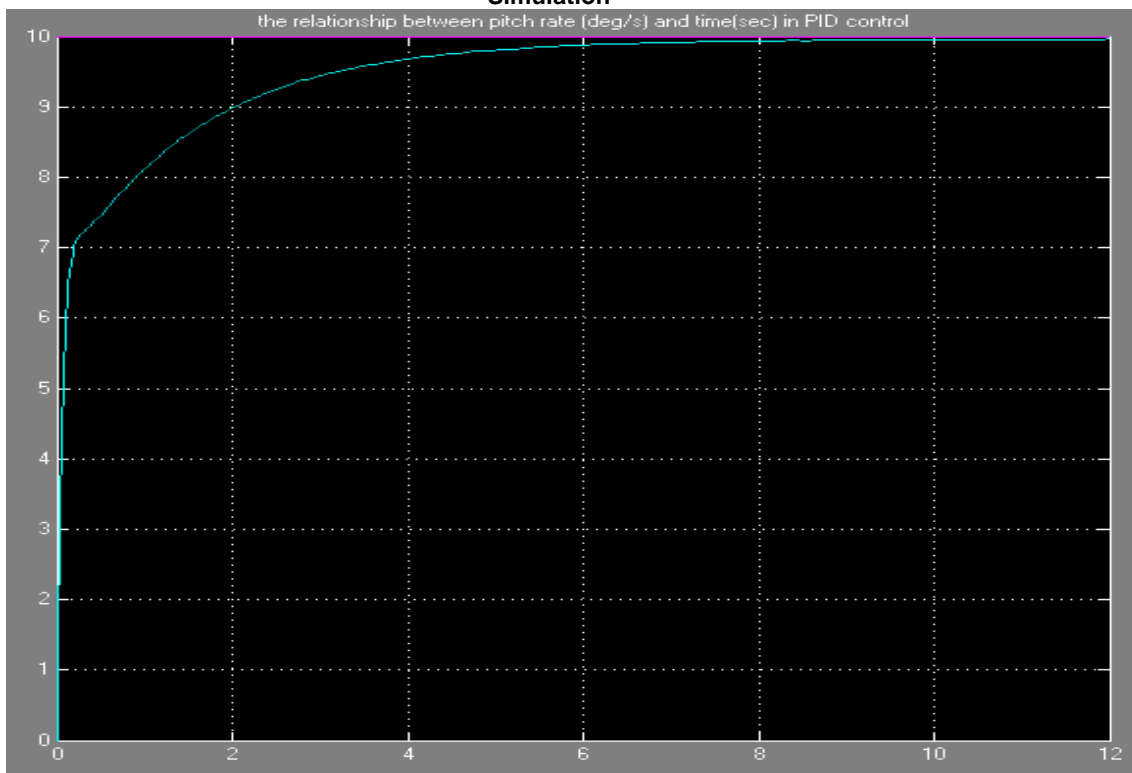


Fig. 18 The relationship between pitch rate (deg/s) y -axis and time (s) x -axis in PID control without noises (response of the control system).

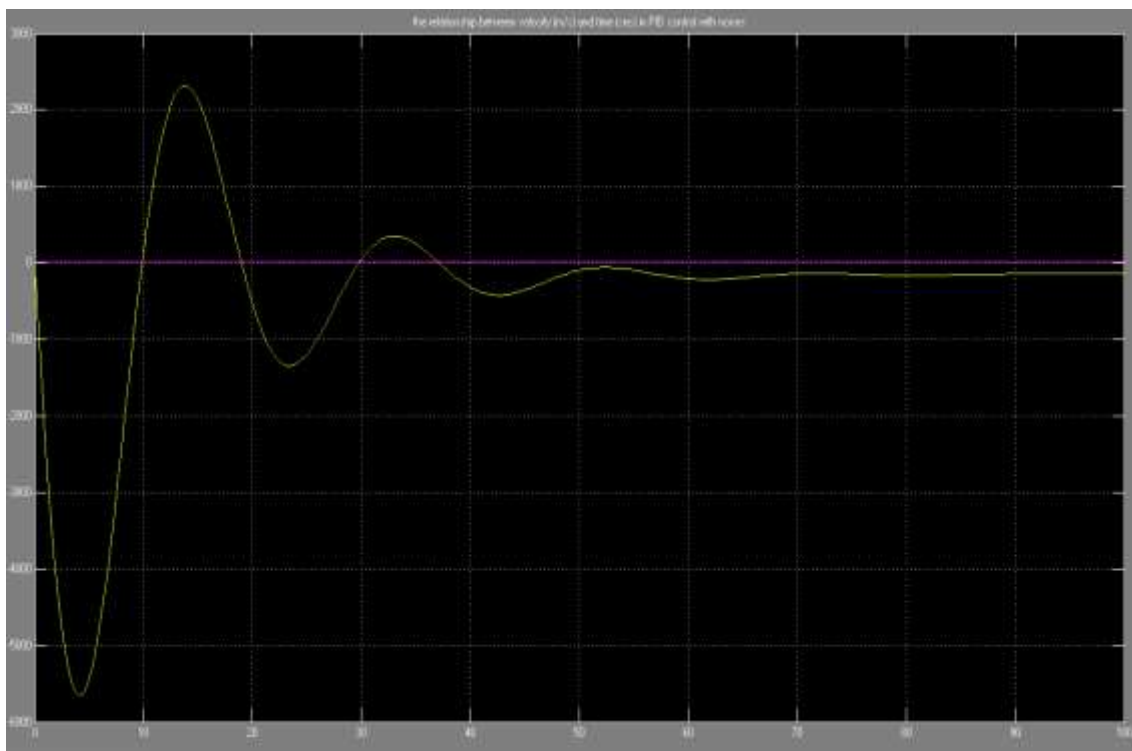


Fig. 19 The relationship between pitch rate (deg/s) y -axis and time (s) x -axis in PID control with noises (response of the control system).

Fig. 21 represents the velocity (m/s) versus time (in seconds) with the system dynamic tuned by LQR and one can easily observe that the resulting UAV has a very slow response (blue lines) compared to the controller red line that presents a faster response. However, there is a significant difference in the proposed dynamic performance between the LQR controller and the PID controller. It demonstrates that system output did not produce an adequate result even when using an LQR controller which is due to an error associated with it, and

the system feedback also may be providing an error to the dynamic system input. Now, with the LQR controller, the UAV system has been obtained with no overshoot, fast rise time, and no steady-state error (blue line).

Evidently, the response of the LQR controller for the dynamic model and analysis of the pitch rate (deg/s) and linear velocity (m/s) of the aircraft system, which are shown in Figs. 20 and 21, were the results of the data obtained from the dynamic UAV aircraft model.

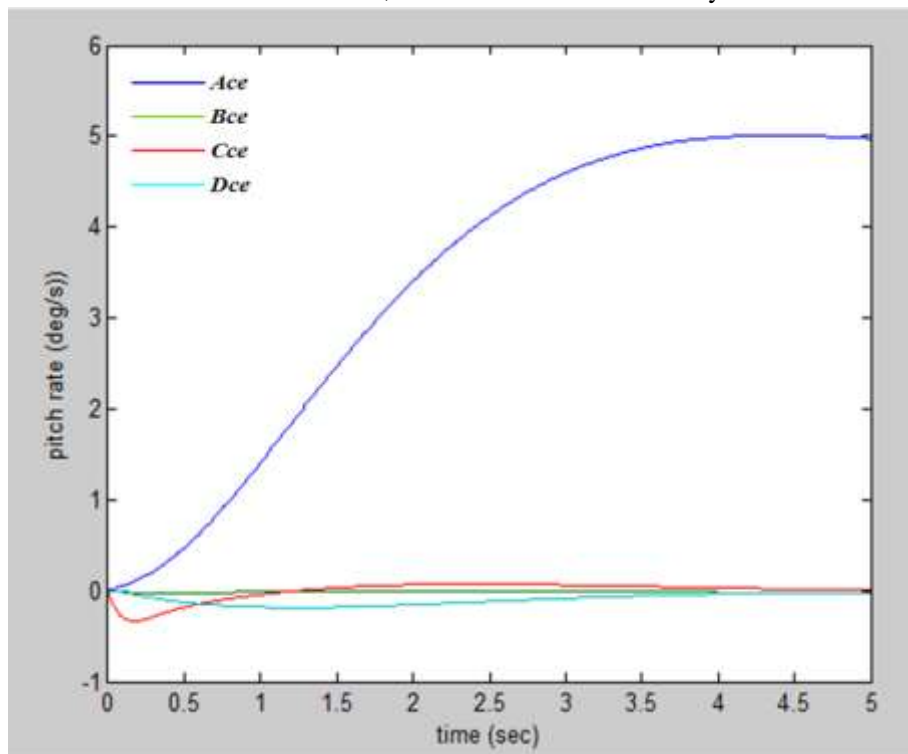


Fig. 20 The relationship between (Comparison results of) pitch rate (deg/s) y-axis and time (s) x-axis s in LQR controller plus observer (Observer design).

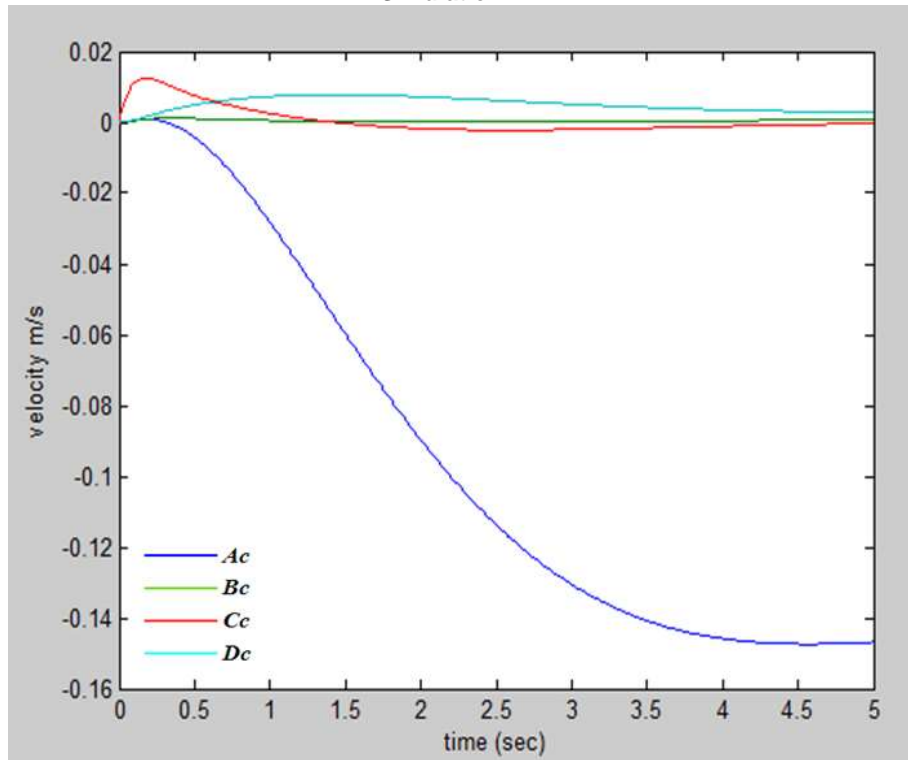


Fig. 21 The relationship between velocity (m/s) y-axis and time (s) x-axis in LQR controller (Full state feedback-LQR design).

In comparing the results of pitch rate (deg/s), the LQR controller may drive the green and red lines to zero, but the average steady-state error after 5 s is not completely driven to zero, and since the LQR is only controlling the pitch rate, the blue line does not converge to zero. Furthermore, from the blue line, the rise time is about 2 s, and the settling time is about 3.5 s and this is in line with the steady-state error. Although it is still large, the design characteristics of the UAV control system are still within the range of acceptable variables for system stability. Clearly, the system is faster in response to the linear velocity and pitch rate state, but the response has an initial oscillation for few seconds. In summary, the UAV system design requirements, i.e., LQR controller requirements, show significant results of overshoot less than 10%, rise time less than 2 s, settling time less than 5 s, and steady-state error less than 2%.

4. Conclusions

This study implements an optimization methodology based on the competitiveness UAV dynamics model

among two different control systems. Any UAV aircraft distributed control system consists of the following important items: electrical equipment components, the functions of the dynamic components, the control system for the dynamic components, a system for detection of failed components, and system failure modes. This means that intelligent technology furnishes practical applications and intelligent systems in agriculture that integrate advanced electronic devices and control systems for agricultural applications. The output of the UAV in hovering and longitudinal flight can be utilized for critical analysis; the PID and LQR controllers demonstrate the reliability to maintain the aircraft position based on maintenance initiatives. It was difficult to control the UAV flight especially if the system had some noises or some disturbances. Some of the controllers in the UAV system were unstable especially when some noise disturbances were added to the UAV design or it had some vibration. Other controllers were stable as shown by the figures in this study. So, making the UAV setpoints PID controllers stable should add some

additional capability to the design. The optimum ranges of the coefficient values of \mathbf{K} , which establish the boundaries of the stability behavior of the UAV aircraft, i.e., no instability in hovering, no overshooting the tolerance limits, and yield both the optimal LQR design for the given system and the capability of forecasting an efficient system function, are:

$$\mathbf{K} = \begin{bmatrix} -0.8938 & -7.3439 & 1.2880 & 18.7708 \\ 0.1440 & 0.4591 & -0.0604 & -1.0876 \end{bmatrix}$$

In practice, with the PID control system, the UAV aircraft transient performance illustrated the ability to tolerate a sudden change in equilibrium, especially when environmental conditions may not be predicted precisely, without losing the ability to hover. K results provide considerable empirical evidence to support the effect of the PID system on controlling the UAV aircraft flight stability as well as aircraft hovering capability. Recognition of the effect of PID controller gains (K_P , K_I , and K_D) is obvious once the UAV aircraft has hovered. Especially at once regarding the ability to rapidly collaborate to counteract the action of various forces, this clearly demonstrates an interactive control system platform. Consistent behavior of a flight dynamics model with respect to sustaining stable longitudinal flight or hovering flight is one of the major determinants of successful maneuvering flight of UAV aircraft.

The consistent performance of these controllers (PID & LQR) provides the ability to accurately compare each platform with other similar controllers, with the overall objective of stable UAV aircraft performance through a perfect response with less time state error. In flying motion analysis, aircraft often encounters a set of variables that make the onset of flight unstable. In general, the main finding of this project is that the time factor is the main determinant of the stability of UAV aircraft, and the beginning of successful hovering (or stable slow flight) is a requirement during agricultural applications whether it is by fixed-wing UAVs or rotary-wing UAVs. Furthermore, flight duration and aircraft stability could be increased with a simultaneous

decrease in the intensity of thrust forces by reducing the aircraft weight with extensive use of carbon composite materials in construction and an adequate set of PID gains.

Either a PID or LQR controller provides a comprehensive control service for all UAV devices. Aircraft observer services cover all correlated parts of the aircraft by matching the output parameters to the desired stability requirements with steady-state of the relevant dynamic system and perfectly balanced response to rapidly reach and sustain steady-state. The results also compared the PID and LQR controllers. The parameter optimization based LQR controller has better gains and steady-state performance than the PID controller. In agriculture application, a perfect control system allows UAVs to carry a payload above their own weight, but not be overburdened, with the possibility of stable flight along with flight duration. The considerable demand for the use of UAV applications and the accurate measurement of the agricultural fields' variables are the most important factors affecting the determination of the recent developments in modern agricultural machinery technology and precision agriculture. In addition, establishing a perfect control system makes the UAV considerably maneuverable and allows it to hover for crop spraying operations. Finally, with UAV aircraft along with PID and LQR control systems, the design, management, and operation of the technology of agricultural machines will change dramatically and society will benefit enormously in the near future. Therefore, these properties are often exploited in the agricultural applications to power UAVs in field operations management.

Acknowledgments

I would like to express my sincere acknowledgment, appreciation, and gratitude to the Deanship of Scientific Research, Researchers Support Services Unit, Agricultural Research Center, and the College of Food and Agriculture Sciences at the King Saud University,

Saudi Arabia, for their moral and technical support and their valuable authoritative advice.

References

- [1] Mazur, M. 2016. "Six Ways Drones Are Revolutionizing Agriculture." *MIT Technology Review*. Posted on July 20, 2016. Accessed on June 17, 2022. <https://www.technologyreview.com/2016/07/20/158748/six-ways-drones-are-revolutionizing-agriculture/>.
- [2] Norasma, C. Y. N., Fadzilah, M. A., Roslin, N. A., Zanariah, Z. W. N., Tarmidi, Z., and Candra, F. S. 2019. "Unmanned Aerial Vehicle Applications in Agriculture." In *IOP Conference Series: Materials Science and Engineering*. Philadelphia: IOP Publishing Ltd., 506. doi: 10.1088/1757-899X/506/1/012063.
- [3] Tokekar, P., Hook, J. V., Mulla, D., and Isler, V. 2013. "Sensor Planning for a Symbiotic UAV and UGV System for Precision Agriculture." In *Proceedings of the IROS 2013: New Horizon, Conference Digest—2013 IEEE/RSJ International Conference on Intelligent Robots and Systems. IEEE International Conference on Intelligent Robots and Systems*, Tokyo, 5321-6. <https://doi.org/10.1109/IROS.2013.6697126>.
- [4] Giles, D. K., and Billing, R. C. 2015. "Deployment and Performance of a UAV for Crop Spraying." *Chemical Engineering Transactions* 44: 307-12. doi: 10.3303/CET1544052.
- [5] Ju, C., and Son, H. 2018. "Multiple UAV Systems for Agricultural Applications: Control, Implementation, and Evaluation." *Electronics* 7 (9): 162. doi: 10.3390/electronics7090162.
- [6] Hasan, K. M., Suhaili, W. S., Shah Newaz, S. H., and Ahsan, M. S. 2020. "Development of an Aircraft Type Portable Autonomous Drone for Agricultural Applications." In *Proceedings of the 2020 International Conference on Computer Science and its Application in Agriculture (ICOSICA)*, Bogor, Indonesia, 1-5. doi: 10.1109/ICOSICA49951.2020.9243257.
- [7] Wang, L., Huang, X., Li, W., Yan, K., Han, Y., Zhang, Y., Pawlowski, L., and Lan, Y. 2022. "Progress in Agricultural Unmanned Aerial Vehicles (UAVs) Applied in China and Prospects for Poland." *Agriculture* 12 (3): 397. <https://doi.org/10.3390/agriculture12030397>.
- [8] Yuan, W., Hua, W., Heinemann, P. H., and He, L. 2023. "UAV Photogrammetry-Based Apple Orchard Blossom Density Estimation and Mapping." *Horticulturae* 9 (2), 266: 1-22. <https://doi.org/10.3390/horticulturae9020266>.
- [9] Radoglou-Grammatikis, P., Sarigiannidis, P., Lagkas, T., and Moscholios, I. 2020. "A compilation of UAV Applications for Precision Agriculture." *Computer Networks* 172: 107148. <https://doi.org/10.1016/j.comnet.2020.107148>.
- [10] Chen, J., Li, D., Jiang, X., and Sun, X. 2006. "Adaptive Feedback Linearization Control of a Flexible Spacecraft, Intelligent Systems Design and Applications." In *Proc. of Sixth International Conference on Intelligent Systems Design and Applications*, 16-18 October 2006, Jinan, China, 225-30. doi: 10.1109/ISDA.2006.253837.
- [11] Salih, A. L., Moghavvemi, M., Mohamed, H. A. F., and Gaeid, K. S. 2010. "Flight PID Controller Design for a UAV Quadrotor." *Scientific Research and Essays* 5: 3360-7.
- [12] Argentim, L. M., Rezende, W. C., Santos, P. E., and Aguiar, R. A. 2013. "PID, LQR and LQR-PID on a Quadcopter Platform." In *Proceedings of the International Conference on Informatics 2013, Informatics Electronics & Vision (ICIEV)*, 1-6.
- [13] Noshahri, H., and Kharrati, H. 2014. "PID Controller Design for Unmanned Aerial Vehicle Using Genetic Algorithm." In *Proceedings of 2014 IEEE 23rd International Symposium on Industrial Electronics (ISIE)*, 213-7. doi: 10.1109/ISIE.2014.6864613.
- [14] Khatoun, S., Gupta, D., and Das, L. K. 2014. "PID & LQR Control for a Quadrotor: Modeling and Simulation." In *Proceedings of International Conference on Advances in Computing 2014, Communications and Informatics (ICACCI)*, New Delhi, India, 796-802. doi: 10.1109/ICACCI.2014.6968232.
- [15] Oktay, T., and Kose, O. 2019. "Dynamic Modeling and Simulation of Quadrotor for Different Flight Conditions." *European Journal of Science and Technology* 15: 132-42. doi: 10.31590/ejosat.507222.
- [16] Nguyen, H. T., Quyen, T. V., Nguyen, C. V., Le, A. M., Tran, H. T., and Nguyen, M. T. 2020. "Control Algorithms for UAVs: A Comprehensive Survey." *EAI Endorsed Transactions on Industrial Networks and Intelligent Systems* 7 (23): 1-11. doi: 10.4108/eai.18-5-2020.164586.
- [17] Chen, Z., and Jia, H. 2020. "Design of Flight Control System for a Novel Tilt-Rotor UAV." *Hindawi-Complexity* 2020: 1-14. Article ID 4757381. <https://doi.org/10.1155/2020/4757381>.
- [18] Yinka-Banjo, C. O., and Ajayi, O. 2019. *Autonomous Vehicles: Sky Farmers: Applications of Unmanned Aerial Vehicle (UAV) in Agriculture*, edited by G. Dekoulis. Rijeka: IntechOpen, 107-28. doi: 10.5772/intechopen.89488. <https://www.intechopen.com/books/autonomous-vehicles/sky-farmers-applications-of-unmanned-aerial-vehicles-uav-in-agriculture>.
- [19] Wang, L., Lan, Y., Zhang, Y., Zhang, H., Tahir, M. N., Ou, S., Liu X., and Chen, P. 2019. "Applications and Prospects of Agricultural Unmanned Aerial Vehicle Obstacle Avoidance Technology in China." *Sensors* 19 (3): 1-16. <https://doi.org/10.3390/s19030642>.

- [20] Kim, J., Kim, S., Ju, C., and Son, H. 2019. "Unmanned Aerial Vehicles in Agriculture: A Review of Perspective of Platform, Control, and Applications." *IEEE Access* 7: 105100-15. doi: 10.1109/ACCESS.2019.2932119.
- [21] Kok, K. Y., and Rajendran, P. 2015. "Enhanced Longitudinal Motion Control of UAV Simulation by Using P-LQR Method." *International Journal of Micro Air Vehicles* 7 (2): 203-10. doi: 10.1260/1756-8293.7.2.203.
- [22] Rahimi, M. R., Hajighasemi, S., and Sanaei, D. 2013. "Designing and Simulation for Vertical Moving Control of UAV System Using PID, LQR and Fuzzy Logic." *International Journal of Electrical and Computer Engineering* 3 (5): 651-9. doi: 10.11591/ijece.v3i5.3440.
- [23] Matlab, MATrix LABoratory. 2022. *MathWorks® Control System Toolbox, R2022b*. Natick: The MathWorks, Inc. <https://www.mathworks.com/help/control/index.html>.
- [24] MacKunis, W., Kaiser, M. K., Patre, P. M., and Dixon, W. E. 2008. "Asymptotic Tracking for Aircraft via an Uncertain Dynamic Inversion Method." In *Proceedings of the 2008 American Control Conference, ThC16.5*, Seattle, June 11-13 2008, WA, USA, 3482-7.
- [25] McCarthy, M. A. 1997. "Simulation in Undergraduate Education (A Case Study Using MATLAB)." In *Proceedings of the Third International Conference on Computer Based Learning in Science*, Leicester, UK, J1-1 to J1-11. doi: 10.13140/RG.2.1.4771.4329.
- [26] Kumar, N., and Jain, S. 2014. "Identification, Modeling and Control of Unmanned Aerial Vehicles." *International Journal of Advanced Science and Technology* 67: 1-10. doi: 10.14257/ijast.2014.67.01.
- [27] Houari, A., Bachir, I., Mohamed, D. K., and Mohamed, M. K. 2020. "PID vs. LQR Controller for Tilt Rotor Airplane." *International Journal of Electrical and Computer Engineering* 10 (6): 6309-18. doi: <http://doi.org/10.11591/ijece.v10i6.pp6309-6318>.
- [28] Kok, K. Y., Rajendran, P., and Wee, L. 2016. "Proportional-Derivative Linear Quadratic Regulator Controller Design for Improved Longitudinal Motion Control of Unmanned Aerial Vehicles." *International Journal of Micro Air Vehicles* 8 (1): 41-50. doi: 10.1177/1756829316638210.
- [29] Ahmed, S. F., Kadir, K., and Joyo, M. K. 2016. "LQR Based Controller Design for Altitude and Longitudinal Movement of Quad-Rotor." *Journal of Applied Sciences* 16 (12): 588-93. doi: 10.3923/jas.2016.588.593.
- [30] Gao, Z., Miklosovic, R., Radke, A., Zhou, W., and Zheng, Q. 2007. "Controllers, Observers, and Applications Thereof." World Intellectual Property Organization, International Bureau, US WO 2007/035559 A2, USA. <https://patents.google.com/patent/WO2007035559A2/en>.
- [31] Gao, Z., Miklosovic, R., Radke, A., Zhou, W., and Zheng, Q. 2011. "Controllers, Observers, and Applications Thereof." U.S. Patent Documents, U.S. Patent No. US 8,060,340 B2, Nov. 15, 2011, Sheet 52 of 52, US 8,060,340 B2, USA. <https://core.ac.uk/download/pdf/10564584.pdf>.
- [32] Saeed, A., Ali, S. U., and Shah, M. Z. 2016. "Linear Control Techniques Application and Comparison for a Research UAV Altitude Control." In *Proceedings of the 13th International Bhurban Conference on Applied Sciences and Technology (IBCAST)*, 12th-16th January 2016, Islamabad, Pakistan. doi: 10.1109/IBCAST.2016.7429866.
- [33] Al-Isawi, M. M. A., Attiya, A., and Adoghe, J. O. 2020. "UAV Control Based on Dual LQR and Fuzzy-PID Controller." *Al-Khwarizmi Engineering Journal* 16 (3): 43-53. doi: 10.22153/kej.2020.08.001.
- [34] Ziegler, J. G., and Nichols, N. B. 1942. "Optimum Settings for Automatic Controllers." *Transactions of the ASME* 64: 759-68.
- [35] Guerrero, J., Pacioselli, C., Pralits, J. O., Negrello, F., Silvestri, P., and Bottaro, A. 2013. "Preliminary Design of a Small-Sized Flapping UAV: II. Aerodynamic Performance and Flight Stability." In *Proceedings of the Conference AIMETA 2013*, Torino, Italy.
- [36] Caughey, D. A. 2011. "Introduction to Aircraft Stability and Control: Course Notes for M&AE 5070." M.Sc. thesis, Cornell University. https://courses.cit.cornell.edu/mae5070/Caughey_2011_04.pdf
- [37] Levine, W. S. 2000. *Control System Fundamentals* (1st ed.). Boca Raton, London, New York: CRC Press, 216. ISBN: 0-8493-0053-3.
- [38] Bolton, W. 2015. *Instrumentation and Control Systems: Frequency Response (Ch. 11)* (2nd Ed.). Amsterdam, the Netherlands: Elsevier Ltd., 252-81. ISBN: 978-0-08-100613-9. <https://www.sciencedirect.com/topics/engineering/phase-crossover-frequency>, doi: <https://doi.org/10.1016/B978-0-7506-6432-5.X5000-1>, <https://doi.org/10.1016/B978-075066432-5/50011-5>.